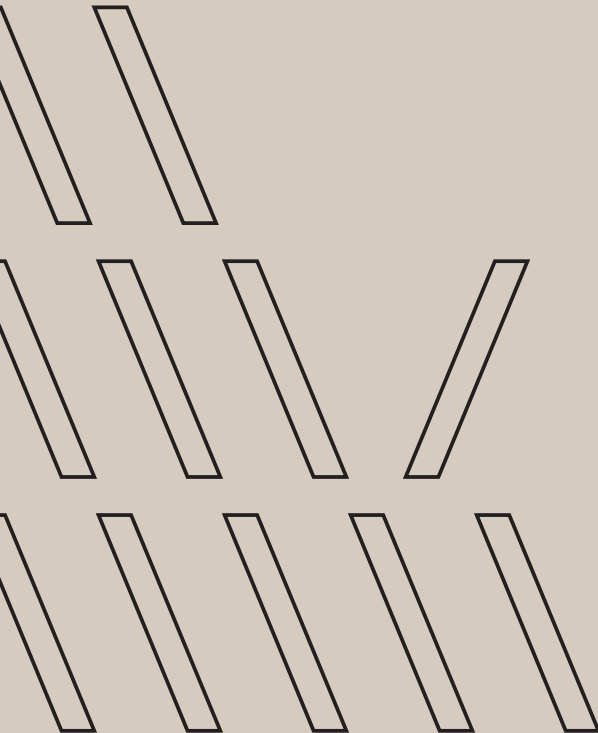


Landslide Modelling & Applications

Workshop on Landslide
Physical and Numerical
Modelling



Editors

Vedran Jagodnik
Josip Peranić
Željko Arbanas (eds.)



Workshop on Landslide Physical and Numerical Modelling

Workshop on Landslide Physical and Numerical Modelling

Vedran Jagodnik, Josip Peranić, Željko Arbanas
Faculty of Civil Engineering, University of Rijeka
Chair of geotechnics

Published by: Faculty of Civil Engineering

University of Rijeka

Rijeka, Croatia

<http://www.modland.uniri.hr>

For publisher : Mladen Bulić, Faculty of Civil Engineering, University of Rijeka

Cover design: Mikser

LaTeX editor: Vedran Jagodnik

Printed in Rijeka by Adriaprint — March 2022

Preface

Physical modelling is widely used research technique despite its limitation. The application of physical modelling on landslides has been a subject of many research in the past. Most of them are based on the use of geotechnical centrifuges which makes possible to use very small models with corresponding gravity enhancement (ng , where n is the scale of acceleration). Despite that, 1g models need not to be neglected. Small scale modelling of landslides at 1g comes with many challenges. One of the main challenge is taking into consideration the low confining stress that usually occurs due to small height of soil layer in a model. Those low confining stresses have an influence on shear stress and strain. Another challenge of 1g models is how to obtain appropriate displacements in 1g conditions. Furthermore, a great consideration has to be made about scaling laws and similarity rules which govern the appropriate scaling factors for data analysis.

The aim of this Workshop is to provide new insights in the behavior of landslides obtained through the research of small scale landslide models at 1g conditions. The more widespread view into available measuring methodologies and techniques leads to further development in the field of physical modelling, especially in the domain of 1g physical models. By sharing the scientific ideas and creative approaches, we hope to provide useful information and insights to the landslide community and facilitate the development of new technologies and methods.

The editors would like to express their sincere gratitude to the authors for sharing their knowledge and experiences in small-scale modelling of landslides at 1g.

The document is divided in two main section sections: (i) monitoring techniques for small scale landslide models, and (ii) numerical modelling of landslides . The first section is covered with three papers entitled "Small-scale physical landslide models under 1g infiltration conditions and the role of hydrological monitoring", "Physical modelling investigation and integrated analysis of landslides for defining risk scenarios" and "Digital image correlation and the use of high-speed cameras for 3D displacement monitoring in 1g small-scale landslide models". The presented papers are focused on the physical modelling of landslides and the use of various techniques and methodologies to measure displacements and water content of soil. The second section, covered with paper "Numerical simulations of landslide physical model results", concerns about the use of advanced numerical modelling to simulate landslide behaviour.

This Workshop is organized in the frame of the Project IP-2018-01-1503 "Physical modelling of landslide remediation constructions behaviour under static and seismic actions (ModLandRemSS)" and supported by Croatian Science Foundation.

Content

| | |
|--|------------|
| Content | vii |
| Small-scale physical landslide models under 1g infiltration conditions and the role of hydrological monitoring | 1 |
| Digital image correlation and the use of high-speed cameras for 3D displacement monitoring in 1g small-scale landslide models | 19 |
| Physical modelling investigation and integrated analysis of landslides for defining risk scenarios | 29 |
| Numerical simulations of landslide physical model results | 41 |
| List of Project publications | 51 |

Small-scale physical landslide models under 1g infiltration conditions and the role of hydrological monitoring

Josip Peranić^{1,*}, Vedran Jagodnik¹, Nina Čeh¹, Martina Vivoda Prodan¹, Sara Pajalić¹, and Željko Arbanas¹

¹University of Rijeka, Faculty of Civil Engineering, Rijeka, Radmile Matejčić 3, Croatia, +38551265943
*josip.peranic@gradri.uniri.hr

Abstract

Despite the considerable progress made in recent decades, there is still a need for a deeper understanding of the physical processes, mechanisms and crucial factors that lead to rainfall-induced landslides. With ongoing climate change affecting the frequency and intensity of meteorological extremes, and the imperatives of continuous urban expansion undoubtedly influencing the frequency and magnitude of landslides, it is no coincidence that the issue of rainfall-induced landslides has received increasing attention from both the scientific community and landslide practitioners in recent decades. Close observation of the hydromechanical response of slopes exposed to different rainfall loads plays a crucial role in understanding the driving mechanisms and factors affecting rainfall-induced landslides. In combination with appropriate monitoring techniques, small-scale physical landslide models can provide accurate insight into the relevant variables under precisely controlled initial and boundary conditions. This paper presents a model platform for physical modelling of scaled slopes under 1g rainfall infiltration conditions, developed at the Faculty of Civil Engineering, University of Rijeka, Croatia, within the four-year research project "Physical modelling of landslide remediation constructions' behaviour under static and seismic actions". Some of the main features of the model platform and the materials used for testing are described. Special attention is given to the sensor network that allows precise monitoring of soil moisture and pore water pressure in a scaled slope during rainfall simulation. Finally, two interesting examples of monitoring data are singled out and analysed with working frameworks relevant to the study of scaled slope models exposed to rainfall.

Keywords: physical modelling, scaled slopes, landslides, rainfall, hydraulic monitoring, sensors

1 Introduction

Landslides are one of the most common geological hazards, usually caused by intense and/or prolonged rainfall. With the ongoing climate change, the continuous expansion of urban areas and the development of infrastructure, the increasing interaction between humans and landslides seems inevitable. It is therefore no coincidence that the issue of rainfall-induced landslides has received increasing attention from both the scientific community and landslide practitioners in recent decades. Despite considerable efforts and progress in understanding the physical processes and mechanisms responsible for triggering rainfall-induced landslides, the issue remains an important topic for the landslide scientific community. Complex physical processes controlling the hydro-mechanical response of slopes during transient infiltration of rainfall, highly non-linear material properties and spatial variations of the soils involved, quantification of time-dependent

boundary conditions, associated hysteresis effects exhibited by the soil as a function of flow direction, and strong spatial and temporal variations in rainfall characteristics are just some of the aspects contributing to the complexity of the problem. Various approaches have been successfully used to study the hydraulic response and failure mechanisms of landslides triggered by a rainfall. For example, numerical models have been used to investigate how different factors affect the stability of both shallow and deep-seated landslides (e.g., [1–10]). Field monitoring has been successfully used to observe the hydraulic and mechanical response of slopes in different geological and climatic contexts (e.g. [11–17]). Particularly valuable data have been obtained from field experiments on instrumented slopes exposed to artificial rainfall or soil moisture increase conditions (e.g. [12, 18–22]). Various laboratory devices have provided useful information on the hydromechanical behaviour of soil samples tested under conditions similar to those found on field slopes during rainfall infiltration (e.g. [23–25]). While size effects, problems associated with taking and testing intact soil samples, and stress conditions and loading paths that cannot fully replicate field conditions are often highlighted as major shortcomings of laboratory sample-size experiments, the interpretation of data from large-scale field experiments can also be complicated by complex soil profile conditions, difficulties in installing monitoring equipment, introducing preferential water flow paths into the slope, etc. Testing small- or large-scale physical landslide models is an additional useful approach that allows accurate observation of the hydraulic and mechanical responses of a slope under precisely controlled initial and boundary conditions. In combination with advanced monitoring techniques and appropriate sensor networks, they have been successfully used, for example, to study the infiltration process, landslide initiation and the propagation phase of landslides triggered by artificial rainfall under 1g conditions (e.g., [9, 26–31]). This paper presents a model platform for physical modelling of small-scale slopes under 1g rainfall conditions developed at the Faculty of Civil Engineering, University of Rijeka, Croatia. The main features and capabilities of the model platform are described, with particular emphasis on the advanced sensor network that enables precise monitoring of the hydraulic response of scaled slopes under simulated rainfall conditions. Two examples of monitoring data are presented and analysed with working frameworks relevant to the study of scaled slope models initiated by rainfall.

2 Physical model

One of the main objectives of the four-year research project "Physical modelling of landslide remediation constructions' behavior under static and seismic actions", which started in October 2018 at the Faculty of Civil Engineering, University of Rijeka, Croatia, was to develop platforms that enable the study of small-scale physical landslide models under static (rainfall) and seismic (earthquake) conditions. The main idea of the Project is to compare the responses of scaled slope models that are built of different soil types and geometric conditions, with and without remediation measures, exposed to different loading conditions. It was expected that the results obtained would provide useful data that could be used to predict the behaviour of real-scale slopes and to improve design procedures and the selection of appropriate landslide remediation measures. The physical model for testing small-scale soil slopes under 1g rainfall infiltration conditions considered in this paper was developed to enable the triggering of landslides by an artificial rainfall. A sensor network consisting of miniature pore water pressure (pwp) and soil moisture sensors allows observation of the hydraulic response of the scaled models, while suitable photogrammetric equipment and accelerometers allow measurement of displacements during a test. The model consists of several main parts, which are briefly described in the following text. A detailed description can be found in [32], [33], and [30]. The model platform itself consists of steel elements and plates with transparent plexiglass side walls that allow the advancement of the wetting front and the onset of displacement to be observed during the experiment. Three basic steel segments, 1 m wide and 0.3 m, 1.4 m and 0.8 m long, form the upper, middle and lower parts of the platform respectively. The joint connections and adjustable height of the upper part allow the models to be built with different inclinations from 20 to 45 degrees. The geogrid attached to the bottom of

the platform prevents the soil from sliding along the impermeable steel plates during the test. Liquid rubber and silicone are used to seal small gaps between plexiglass walls and perforations in the structure to ensure that the model is watertight during a test. Drainage pipes inserted through the plexiglass in the lower part of the model allow the water level to be controlled during the test and the water to be drained after the test. The empty platform before the installation phase is shown in Fig. 1a.



Figure 1: Details from the model construction phase: a) The empty model platform; b) Compaction of the soil material and installation of the measuring instruments; c) Scaled slope model with installed measuring instruments before the start of the test.

2.1 Model construction and soil properties

The platform is suitable for any soil type and installation at any predefined conditions in terms of initial density and moisture content. Any of the appropriate standard laboratory methods commonly used to install soil samples in conventional soil testing laboratory equipment can be used to create the model at the desired density or moisture content. The results presented in this study were obtained on two different soil materials, which are described in the following text. A fine-grained sand was used as the base soil and the simplest soil material. Another soil type was obtained by adding 15% by weight of kaolin clay to a clean sand (hereafter referred to as SK15). The clean sand was installed at 50% of the relative density ($D_{r,i}$) and at 2% of the initial moisture content (w_i), while the $D_{r,i}$ and w_i were 75% and 8.1% for the SK15, respectively. For both soil materials, Ladd's method [34] of under-compaction was used to construct 30 cm deep slope models. This involved compaction of 5 layers of soil, each 6 cm high, and attempting to achieve as homogeneous conditions as possible in terms of density and soil moisture distribution (Fig. 1b). After the model was built, the entire model was covered with nylon to prevent excessive drying due to evaporation until the start of the test (Fig. 1c). Tab. 1 shows the basic soil properties of the previously described soils.

Table 1: Basic soil properties of sand and sand with 15 % kaolin by mass (SK15) with the target initial conditions.

| Parameter (unit) | Material | |
|-------------------------------------|----------|----------|
| | Sand | SK15 |
| Specific gravity, G_s | 2.7 | 2.67 |
| Effective particle size | | |
| D_{10} (mm) | 0.19 | 0.056 |
| D_{60} (mm) | 0.37 | 0.207 |
| Uniformity coefficient, c_u | 1.95 | 54.11 |
| Minimum void ratio, e_{min} | 0.64 | 0.54 |
| Maximum void ratio, e_{max} | 0.91 | 1.43 |
| Hydraulic conductivity, k_s (m/s) | 1.00E-05 | 3.50E-06 |
| Friction angle, ϕ ($^\circ$) | 34.9 | 31.8 |
| Cohesion, c (kPa) | 0 | 4.4 |
| Initial porosity, n_i | 0.44 | 0.43 |
| Initial relative density, D_{ri} | 0.5 | 0.75 |
| Initial water content, w_i (%) | 2 | 8.1 |

2.2 Rainfall simulator

In addition to the hydraulic properties of the soil, the rainfall characteristics play a decisive role when it comes to rainfall-induced landslides. The development of the rainfall simulator that meets the specific requirements of the Project was an important step in the early stages of developing a small-scale physical landslide model. In particular, the ability to apply a wide range of rainfall intensities depending on the soil material tested and the specific objectives of the experiment, sufficient spatial uniformity of the simulated rainfall and the ability to modify rainfall patterns and characteristics, preventing excessive erosion due to raindrop impact forces (which are closely related to the diameter of simulated raindrops, impact velocity and/or water pressure), the portability of the rainfall simulator due to its possible use not only with the platform for testing under static conditions but also under dynamic conditions, and the limited budget available for the construction of the simulator were the main considerations in the design and construction of the rainfall simulator. The rainfall simulator developed consists of three independent branches that deliver water from the main control block to the spray nozzles. The main control block is connected to a water supply and consists of the control units that regulate the intensity and work of the rainfall simulator, such as pressure regulators, manometers, flow meters, filters, etc. High-density polyethylene pipes convey the pressurised water from the control block to three sprinkler branches, which are adjustable in height and equipped with various spray nozzles (Fig. 2). At the reference pressure of 2 bar, the axial-flow full-cone nozzles (Tab. 2) can produce intensities ranging from less than 30 mm/h to more than 150 mm/h. The setup can be easily modified to achieve any other desired rainfall intensity or pattern.

2.3 Monitoring equipment

The monitoring equipment can be divided into two main parts: i) geodetic monitoring system based on innovative photogrammetric equipment for multitemporal landslide analysis [35] of image sequences obtained from a pair of high-speed stereo cameras [36] and terrestrial laser scanning and structure-from-motion (SfM) photogrammetry surveys that allow the determination of the surface model of the slope in the pre- and post-failure phase [37]; ii) geotechnical monitoring system consisting of a network of miniature sensors to measure changes in soil moisture, pwp, soil temperature and electrical conductivity, displacements, etc. The ARAMIS is an optical, non-contact 3D measurement system (GOM GmbH) that provides the entire workflow from taking measurements to analysing the data and displaying the results. A set of two



Figure 2: Simulated rainfall with an intensity of 23 mm/h with a detail of the sprinkler branch with axial flow full-cone nozzles.

Table 2: Technical characteristics of full-cone nozzles used to simulate rainfall: spray angle and flow rates (v) for different working pressures (p) (lechler.com).

| Spray angle | Type | v (l/min) | | | |
|-------------|---------|-----------|------|------|------|
| | | p (bar) | | | |
| | | 1 | 2 | 3 | 5 |
| 60° | 490.404 | 0.76 | 1 | 1.18 | 1.44 |
| 60° | 490.444 | 0.95 | 1.25 | 1.47 | 1.8 |
| 60° | 490.484 | 1.21 | 1.6 | 1.88 | 2.31 |
| 60° | 490.524 | 1.52 | 2 | 2.35 | 2.89 |
| 90° | 460.524 | 0.3 | 0.4 | 0.47 | 0.58 |

4-megapixel and two 12-megapixel high-speed cameras is used for multitemporal analysis of landslides from captured stereo image sequences. The system allows continuous monitoring of the 3D coordinates of reference points through all stages of the activity of scaled landslide models. The terrestrial laser scanner FARO Focus 3D X 130 (FARO Technologies Inc.) is used to capture the high-resolution 3D model surface before the start and at the end of the test. The scanner uses phase shift technology to accurately determine the relative 3D position of the scanned points, while reference points are used to overlap the scanned areas and define the relative coordinate system. A Nikon D500 camera with an ultra-wide angle Tokina AT-X 11-20 lens is used for the SfM photogrammetry survey of the physical models. This technique allows the creation of 3D models from multiple overlay images taken at different triangulation angles. Fig. 3 shows the mentioned equipment, a detailed technical description can be found in [30]. The geotechnical monitoring system consists of a complex network of miniature sensors equivalent to the equipment used for field monitoring. All sensors are connected to data loggers that allow continuous data collection of soil moisture, positive pwp and soil suction, displacement, etc. As the focus of this presentation is on the role of hydraulic monitoring of scaled slopes, the measuring devices are described in more detail in the following section.

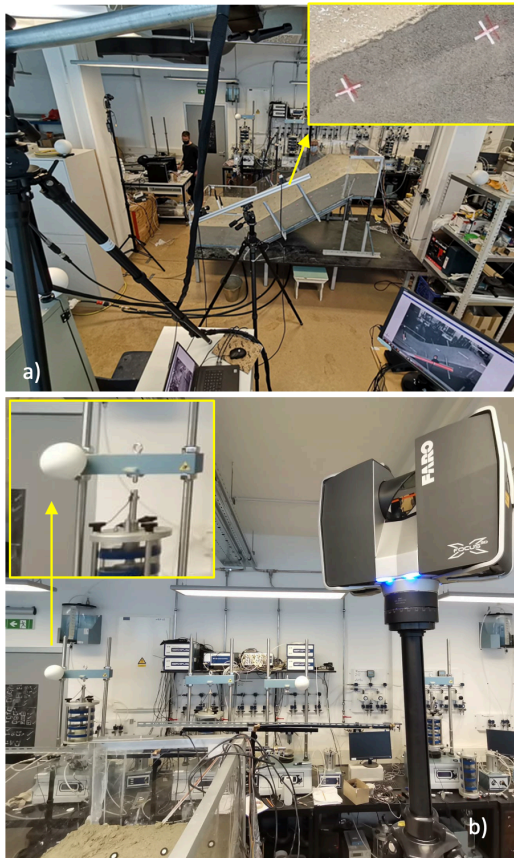


Figure 3: Geodetic monitoring equipment: a) A view of the model from the ARAMIS measuring system (GOM GmbH) and a detail of the (front) 12 megapixel camera monitoring displacements through the plexiglass wall; b) The FARO Focus 3D X 130 (FARO Technologies Inc.) terrestrial laser scanner and a detail of the position of the reference sphere.

3 Equipment for monitoring the hydraulic response

Accurate monitoring of the hydromechanical response of scaled slopes under controlled initial and boundary conditions provides valuable information on the variables controlling the instability phenomena of rainfall-induced landslides. The development of a suitable sensor network for the test conditions and the selection of appropriate measurement techniques are therefore crucial steps in the development of small-scale physical landslide models. The following part describes the main components that make up the hydrological monitoring system of the physical model. There were several requirements that were considered in the selection of the measurement equipment. Firstly, information on soil moisture and changes in pwp had to be available at appropriate time intervals, which necessitated the use of digitised sensors in combination with suitable data loggers. Secondly, the Project envisaged testing a wide range of soils, from sand to clay. Therefore, the selected measurement equipment had to be able to cover a wide measurement range

occurring in different soil textures, while ensuring sufficient precision, resolution, and responsiveness. The solution was found in the capacitance-based soil water content sensors, which provide rapid detection of changes in soil volumetric water content (VWC) for a wide range of soil textures and conditions, and in the simultaneous use of mini tensiometers for rapid measurement of pwp and matric suction values within the measurement range of standard tensiometers. The soil water potential sensors based on the dielectric constant measurement method were intended for measurements in soils where high soil suction values are expected. Another consideration concerns data redundancy: data had to be collected simultaneously at several depths and along different profiles in order to obtain a complete picture of the temporal-spatial evolution of the different variables during the experiment. Finally, the chosen monitoring equipment should be used in both the small-scale physical landslide models for testing under static (rainfall) and seismic (earthquake) conditions.

3.1 Sensors for measuring the water content of the soil

The TEROS 10 and TEROS 12 are soil moisture sensors from METER Group (Inc.) for indirect measurement of the VWC of porous materials. Both sensors are based on the capacitance method for predicting the amount of water in the soil based on the electrical properties of the soil and the calibration procedure proposed by Topp et al. [38]. An electromagnetic field (70 MHz oscillating wave) is used to measure the apparent dielectric permittivity (ϵ_a) of the soil. The sensor delivers an oscillating wave to sensor needles that charge according to the dielectricity of the material. The charging time is proportional to the dielectricity of the substrate and the VWC of the substrate (TEROS 10 manual [39]). Depending on the measured charging time, a microprocessor outputs a raw sensor value (RAW) based on the substrate ϵ_a . Finally, a calibration equation specific to the substrate is used to convert RAW values to VWC values. The high measurement frequency ensures insensitivity to variations in soil texture and electromagnetic conductivity (TEROS 10 manual [39]). In all tests, a generic calibration equation from the manufacturer for mineral soils was used to predict VWC, based on the RAW output of the METER data logger ZL6:

$$\Theta = 4.824 \cdot 10^{-10} \cdot RAW^3 - 1.222 \cdot 10^{-6} \cdot RAW^2 + 2.855 \cdot 10^{-3} \cdot RAW - 2.154 \quad (1)$$

For RAW outputs from the METER data logger, the apparent dielectric permittivity can be used to determine VWC, e.g., with the Topp's equation [38]:

$$\epsilon = 1.054 \cdot 10^{-4} \cdot e^{2.071 \cdot 10^{-3} \cdot RAW} \quad (2)$$

TEROS 10 has a VWC range for mineral soils of 0.00-0.64 m³/m³ with a resolution of 0.001 m³/m³ and an accuracy of ± 0.03 m³/m³ in mineral soils with a solution EC < 8 dS/m (TEROS 10 manual [39]). On the other hand, TEROS 12 has a slightly larger VWC measurement range (0.00-0.70 m³/m³) with the same resolution and accuracy as TEROS 10. The temperature range for TEROS 12 is -40 to 60 °C, with a resolution of 0.1 °C and a measurement accuracy of ± 1 °C. The measuring range of the TEROS 12 for total electrical conductivity is 0-20 dS/m with a resolution of 0.001 dS/m and a measuring accuracy of $\pm 3\%$ (TEROS 12 manual [40]). The volume of the measuring sensitivity of the TEROS 12 with 1010 mL is significantly larger than the measuring volume of the TEROS 10 with 430 mL (Fig. 4). Fig. 5 shows some details on the installation and calibration of the sensors.

3.2 Sensors for measuring the water potential of the soil

At some point in the development of the Project, standard tensiometers with vacuum gauges (IR -45 and T1) and digital (TEROS 32) tensiometers, mini tensiometers (TEROS 31) and TEROS 21 soil water potential sensors were purchased to measure soil water potential, depending on project needs and available funds.

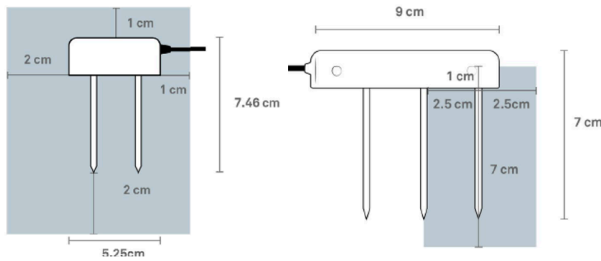


Figure 4: Influence volume for VWC measurements with TERSO 10 (left) and TERSO 12 (right) sensors (TERSOS manual).



Figure 5: Installation of TERSO 10 during model build-up (left) and calibration for clean sand.

The non-digitised standard tensiometers IR -45 (Irrometer Company, Inc.) and T1 (MMM Tech Support GmbH & Co. KG) were already purchased in the initial phase of the Project and used for the first test on clean sand (Fig. 6a). The TERSO 32 (Fig. 6b) and TERSO 31 (Fig. 6c) digitised tensiometers (METER Group, Inc.) were procured in the later stages of the Project and used with ZL6 data loggers from METER to continuously record measurements at time intervals of up to 1 minute in other soil materials. The TERSO 21 (METER Group, Inc.) sensors were intended to be used in a measurement range beyond that of standard (mini) tensiometers. In addition to good hydraulic contact of the ceramic with the surrounding soil, which is necessary for accurate measurement of all the above sensors, the tensiometers must be appropriately conditioned before insertion into the soil to achieve the full measuring range and a fast response during the equilibration phases. TERSO 21 is a maintenance-free matric potential sensor designed for long-term, continuous field measurements (TERSOS 21 manual [41]). It uses a similar approach as the VWC sensors TERSO 10 and TERSO 12: The sensor measures the ϵ_a of a solid matrix (porous ceramic discs) to determine its water content. Since the ϵ_a of porous ceramic discs strongly depends on the amount of water present in the pore spaces and the porous ceramic discs tend to reach a hydraulic equilibrium with the surrounding soil, the measured water content of the solid matrix is used to determine the water potential of the soil based on a known soil water retention curve (SWRC) of porous stones. The measuring range for the water potential of the TERSO 31 mini-tensiometer is -85 to +50 kPa with a resolution of ± 0.0012 kPa and an accuracy of ± 0.15 kPa. It also provides temperature measurements in the range of -30 to +60 °C with a resolution of ± 0.01 °C and an accuracy of ± 0.5 °C. The TERSO 21 has a measuring range of -9 to -100 000 kPa for water potential and -40 to 60 °C for soil temperature.

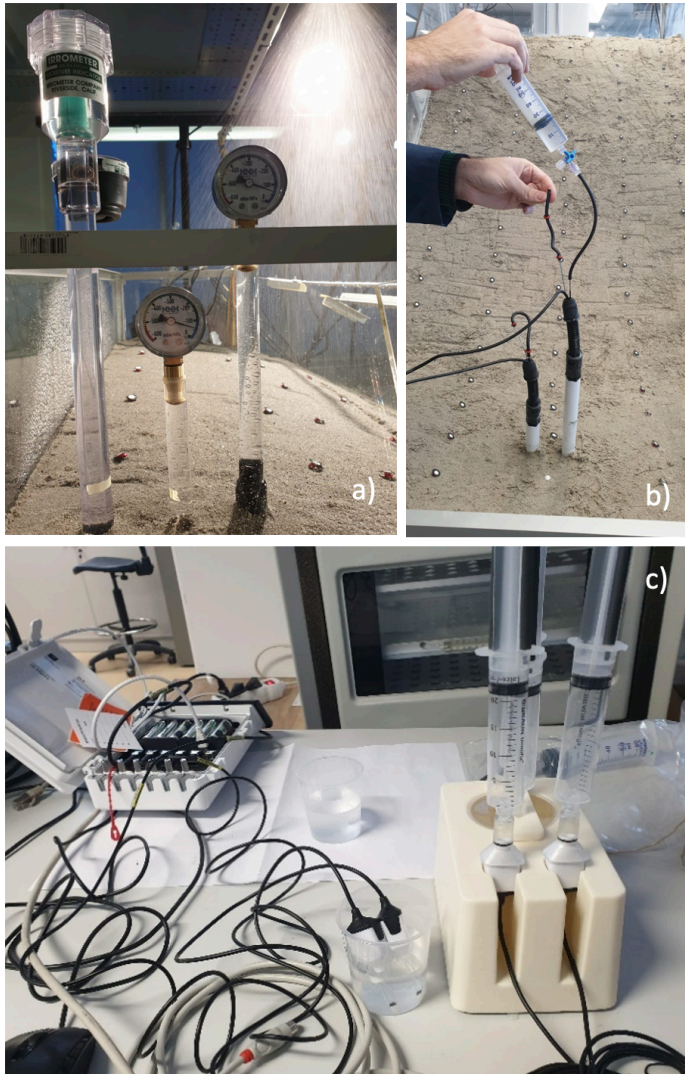


Figure 6: a) Standard, non-digitised IR and T1 tensiometers; b) preconditioning of TERSO 32; and c) TERSO 31 tensiometers.

4 Examples of measurement and data analysis

This section presents some examples of hydraulic monitoring results for different soil materials, geometric, initial and boundary conditions. The results are interpreted in the context relevant to the study of the mechanisms and factors driving the instability of rainfall-induced landslides. For two different soil materials and tests, particular details were singled out and discussed in detail.

4.1 Example 1: Initiation of a sandy slope due to the rise of the groundwater level (GWL)

The first example considers the case of the initiation of a scaled slope built of clean sand with a slope of 35° , subjected to a constant rainfall intensity of 72.6 mm/h until the occurrence of the first instability in the form of a small rotational landslide at the toe of the slope. After the first slide, further instabilities developed in the form of retrogressive slides up to the top of the slope. Fig. 7 shows images taken by the Aramis system at the beginning of the test, together with measurement profiles in the upper (H), middle (M) and lower (L) parts of the model (a); 49 minutes after the start of the rainfall, when the first traces of GWL reaching the surface in the central part of the base are visible (yellow square in Fig. 7a) (b); 51 minutes after the start of the rainfall, when the entire base is submerged (c); and 56 minutes after the start of the rainfall simulation (d), when the first small rotational landslide occurs at the toe of the slope (bottom right in (d)).

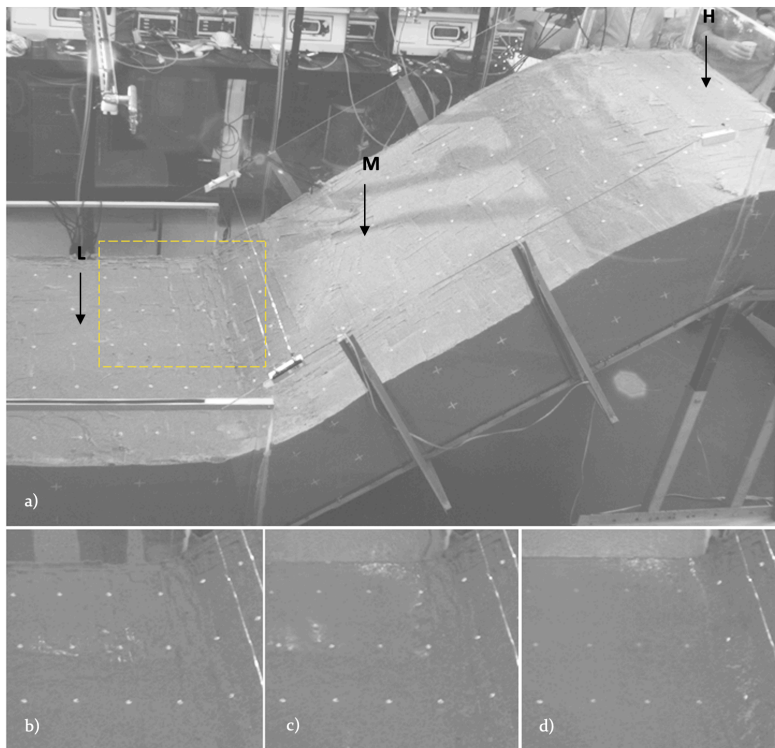


Figure 7: Test with clean sand inclined at 35° , taken with the Aramis system: At the beginning of the test with measurement profiles in the upper (H), middle (M) and lower (L) sections of the slope, respectively (a); 49 minutes after the start of the rainfall: the first traces of GWL reaching the surface in the middle part of the base (b); 51 minutes after the start of the rainfall: the entire base is submerged (c); The first small rotational landslide at the foot of the slope (bottom right), 56 minutes after the start of the rainfall simulation.

For the same test, the VWC values measured with TEROS 10 and TEROS 12 sensors at the base of the model (L) are shown in Fig. 8. The measurement results indicate that the GWL reaches the sensors installed at 24, 18 and 12 cm after about 23, 39 and 41 minutes, respectively. The readings become

constant (indicating saturated conditions) and the maximum value is reached after about 48 minutes at a depth of 6 cm, which is exactly in line with the observations during the experiment and timing reported in Fig. 7. This indicates that, despite certain deviations in the absolute reading values, which could be due to various reasons such as requirements on the calibration procedure of each sensor, different readings of the TEROS 10 and TEROS 12 sensors or different soil densities achieved around the moisture probes, or unequal conditions in terms of contact and presence of gaps between the surrounding soil and the needles of the sensor, can provide useful data on the trend of soil moisture increase in general, providing information on the saturation state during the infiltration process.

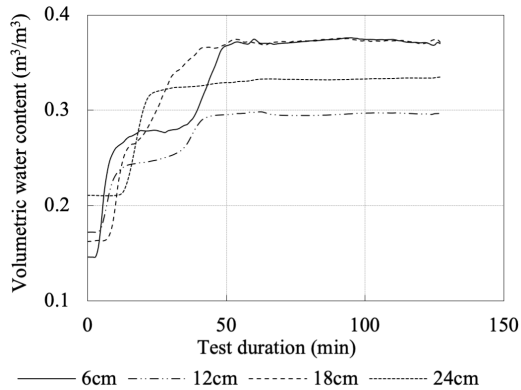


Figure 8: VWC values measured with TEROS10 and TEROS12 sensors at the base (L) section of the model at 6, 12, 18 and 24 cm depth in Example 1.

4.2 Example 2: Hydraulic pathways and a reduction in the shear strength of the soil due to infiltration

The second example deals with the hydraulic paths and stress states experienced by the scaled 40° slope of SK15 material under simulated rainfall conditions. In this test, the continuous rainfall intensity of 20.5 mm/h was interrupted by 10-minute breaks to observe the hydraulic response of the soil (Fig. 9). The numerical markers in Figs. 9 to 12 serve as reference points to follow the course of the experiment and the simulated rainfall conditions when the data are presented in different forms and planes. The number "1" marks the beginning of the experiment, i.e. the start of the rainfall simulation for the first 30 minutes. The numbers "2" and "3" mean that all three nozzles are closed and that the rainfall is stopped for 10 minutes. After that, the rainfall simulation continues for the next 30 minutes with the same intensity as in the previous phase of the test. The number "4" represents the start of another 10-minute rainfall break. Finally, the number "5" indicates the point in the test where the end has been declared and the rainfall simulation has ended. For the sake of brevity, the hydraulic path in Figs. 10 and 11 is shown only for one monitoring point (M-6) located at 6 cm depth in the middle section of the model (M-profile - the same analogy as in Example 1 is used, i.e., see Fig. 7a). As the monitoring point was equipped with a pair of TEROS 10 and TEROS 31 sensors, both the changes in pwp (or matric suction) and VWC are available throughout the test.

Fig. 12 shows how infiltration of rainfall affects the shear strength of the soil by reducing the effective stresses at measurement point M-6. The initial stress state and corresponding shear strength, located on the right-hand side of the path, reflect the soil moisture conditions at the start of the test, most of which are reached during model construction and kept constant until the start of the test. With the onset of rainfall infiltration, the VWC increase and dissipation of the matric suction take place in the form of a transient

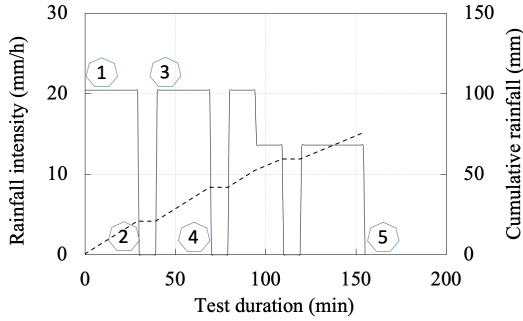


Figure 9: Simulated rainfall in Example 2.

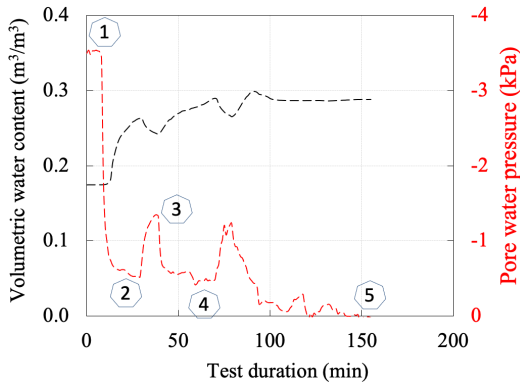


Figure 10: Pwp (matric suction) and VWC values measured at 6 cm depth in the middle (M) section during the test in Example 2.

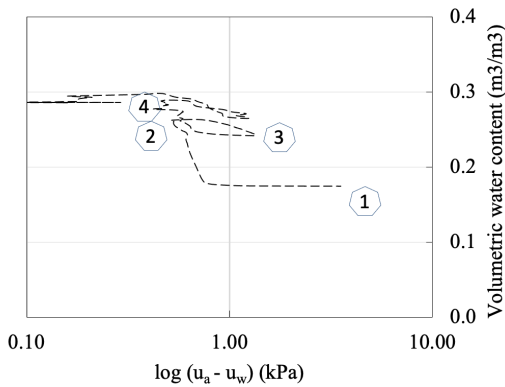


Figure 11: Hydraulic response in $\log (u_a - u_w)$ vs. VWC plane for measuring point M-6 during the test in Example 2.

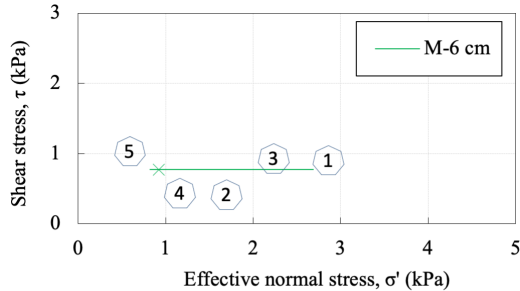


Figure 12: Stress path calculated with Eq. (3) that the monitored point M-6 undergoes during the rainfall infiltration from the Example 2.

process (Fig. 10; "1"- "2"). If a simplified assumption is made that capillarity is the only retention mechanism, a reduction in effective stress during rainfall infiltration can be quantified from the VWC and pwp values observed during the experiment, using, for example, the equation for effective stress by Bishop [42]:

$$\sigma' = \sigma - u_a + \chi \cdot (u_a - u_w) \quad (3)$$

where the effective stress parameter χ is set equal to the effective degree of saturation. For the residual VWC set to $\Theta_r = 0.05$ m³/m³ (an assumption based on observations from other tests on SK15 soil material) and the saturated VWC is set to $\Theta_s = 0.3$ m³/m³ (according to the VWC measurements in Fig. 10), the monitored values result in a stress path shown in Fig. 12. Movement from right to left indicates that the matric suction is dissipating, and saturation is increasing. The cross on the left side of the path indicates the effective stress at the observed point at the beginning of the test, without taking into account the correction of the effective stress for unsaturated soil conditions, i.e., as defined in Terzaghi's effective stress equation.

5 Discussion and concluding remarks

This paper presented a newly developed platform for physical modelling of small-scale slopes under 1g rainfall conditions, developed at the Faculty of Civil Engineering, University of Rijeka, Croatia, as part of a four-year research project "Physical modelling of landslide remediation constructions' behaviour under static and seismic actions". The main features of the platform and its main components, namely the monitoring equipment and the rainfall simulator, as well as the characteristics of the soil materials used for the construction of the scaled slopes are presented. Since the focus of the paper was on monitoring the hydraulic response of scaled slope models, special attention was given to the sensor network that allows monitoring soil moisture and pore water pressure changes during rainfall simulation. Among the many results obtained through the various research activities of the Project, two interesting examples were singled out to analyse hydrological monitoring data in the context of instability mechanisms of scaled slopes exposed to simulated rainfall. The first example showed how monitoring changes in soil moisture can provide accurate (apparently also instantaneous) insights into the different stages of moisture content increase during the different phases of transient infiltration as well as the subsequent GWL rise. These results are placed in the context of the initiation of a scaled sandy slope due to the GWL rise. The data on the observed hydraulic response, known initial and boundary conditions can be used as valuable tools for establishing relationships in a scaled slope model, an investigation of the conditions and mechanisms leading to slope failure. In the second example, the hydraulic paths exhibited by the scaled slope of a sand mixture with 15% kaolin content during a simulated rainfall were investigated. The results show how simultaneous observation of VWC and

pore water pressure, when embedded in appropriate working concepts, can provide valuable insights into the hydraulic paths and effective stress states experienced by the model during tightly controlled infiltration conditions during rainfall. Results interpreted in the $\log(u_a - u_w)$ vs. VWC plane for the monitored point indicate that the soil exhibits hysteresis effects as it undergoes multiple drying-wetting cycles (e.g., points 2-3-4 in Fig. 11). This suggests the possibility of using small-scale physical slope models to investigate the role of hydraulic hysteresis effects on the behaviour of slopes under different rainfall patterns, in general.

Acknowledgements

The research presented in this paper was supported by Croatian Science Foundation under the Project IP-2018-01-1503 "Physical modelling of landslide remediation constructions behaviour under static and seismic actions (ModLandRemSS)". This work has been supported in part by Ministry of Science, Education and Sports of the Republic of Croatia under the project Research Infrastructure for Campus-based Laboratories at the University of Rijeka, number RC.2.2.06-0001. The project has been co-funded from the European Fund for Regional Development (ERDF). These supports are gratefully acknowledged. The authors would like to thank laboratory technician Juraj Stella for his help in conducting the tests.

References

- [1] N. Casagli, S. Dapporto, M. L. Ibsen, V. Tofani, and P. Vannocci, "Analysis of the landslide triggering mechanism during the storm of 20th–21st November 2000, in Northern Tuscany," *Landslides*, vol. 3, no. 1, pp. 13–21, Mar. 2006.
- [2] A. Rahimi, H. Rahardjo, and E.-C. Leong, "Effect of Antecedent Rainfall Patterns on Rainfall-Induced Slope Failure," *Journal of Geotechnical and Geoenvironmental Engineering*, vol. 137, no. 5, pp. 483–491, May 2011.
- [3] L. Comegna, L. Picarelli, E. Bucchignani, and P. Mercogliano, "Potential effects of incoming climate changes on the behaviour of slow active landslides in clay," *Landslides*, vol. 10, no. 4, pp. 373–391, Aug. 2013.
- [4] A. Leung and C. Ng, "Analyses of groundwater flow and plant evapotranspiration in a vegetated soil slope," *Canadian Geotechnical Journal*, vol. 50, no. 12, pp. 1204–1218, Dec. 2013.
- [5] L. Cascini, G. Sorbino, S. Cuomo, and S. Ferlisi, "Seasonal effects of rainfall on the shallow pyroclastic deposits of the Campania region (southern Italy)," *Landslides*, vol. 11, no. 5, pp. 779–792, Oct. 2014.
- [6] P. Lollino, F. Cotecchia, G. Elia, G. Mitaritonna, and F. Santaloia, "Interpretation of landslide mechanisms based on numerical modelling: two case-histories," *European Journal of Environmental and Civil Engineering*, vol. 20, no. 9, pp. 1032–1053, Oct. 2016.
- [7] E. Hinds, N. Lu, B. Mirus, and A. Wayllace, "Effects of Infiltration Characteristics on Spatial-Temporal Evolution of Stability of an Interstate Highway Embankment," *Journal of Geotechnical and Geoenvironmental Engineering*, vol. 145, no. 9, p. 05019008, Sep. 2019.
- [8] S. Kang, S.-E. Cho, B. Kim, and G.-H. Go, "Effects of Two-Phase Flow of Water and Air on Shallow Slope Failures Induced by Rainfall: Insights from Slope Stability Assessment at a Regional Scale," *Water*, vol. 12, no. 3, p. 812, Mar. 2020.

- [9] P. Marino, G. F. Santonastaso, X. Fan, and R. Greco, "Prediction of shallow landslides in pyroclastic-covered slopes by coupled modeling of unsaturated and saturated groundwater flow," *Landslides*, vol. 18, no. 1, pp. 31–41, Jan. 2021.
- [10] J. Peranić, S. Mihalić Arbanas, and v. Arbanas, "Importance of the unsaturated zone in landslide reactivation on flysch slopes: observations from Valići Landslide, Croatia," *Landslides*, vol. 18, no. 12, pp. 3737–3751, Dec. 2021.
- [11] R. Greco, L. Comegna, E. Damiano, A. Guida, L. Olivares, and L. Picarelli, "Hydrological modelling of a slope covered with shallow pyroclastic deposits from field monitoring data," *Hydrology and Earth System Sciences*, vol. 17, no. 10, pp. 4001–4013, Oct. 2013.
- [12] S. Springman, A. Thielen, P. Kienzler, and S. Friedel, "A long-term field study for the investigation of rainfall-induced landslides," *Géotechnique*, vol. 63, no. 14, pp. 1177–1193, Nov. 2013.
- [13] M. Bordoni, C. Meisina, R. Valentino, N. Lu, M. Bittelli, and S. Chersich, "Hydrological factors affecting rainfall-induced shallow landslides: From the field monitoring to a simplified slope stability analysis," *Engineering Geology*, vol. 193, pp. 19–37, Jul. 2015.
- [14] A. K. Leung and C. W. W. Ng, "Field investigation of deformation characteristics and stress mobilisation of a soil slope," *Landslides*, vol. 13, no. 2, pp. 229–240, Apr. 2016.
- [15] P. Chen, N. Lu, G. Formetta, J. W. Godt, and A. Wayllace, "Tropical Storm-Induced Landslide Potential Using Combined Field Monitoring and Numerical Modeling," *Journal of Geotechnical and Geoenvironmental Engineering*, vol. 144, no. 11, p. 05018002, Nov. 2018.
- [16] K.-S. Kim, S.-W. Jeong, Y.-S. Song, M. Kim, and J.-Y. Park, "Four-Year Monitoring Study of Shallow Landslide Hazards Based on Hydrological Measurements in a Weathered Granite Soil Slope in South Korea," *Water*, vol. 13, no. 17, p. 2330, Aug. 2021.
- [17] K. Sattler, D. Elwood, M. T. Hendry, D. Huntley, J. Holmes, P. B. Wilkinson, J. Chambers, S. Donohue, P. I. Meldrum, R. Macciotta, and P. T. Bobrowsky, "Quantifying the contribution of matric suction on changes in stability and displacement rate of a translational landslide in glaciolacustrine clay," *Landslides*, vol. 18, no. 5, pp. 1675–1689, May 2021.
- [18] D. M. Krzeminska, T. A. Bogaard, T.-H. Debieche, F. Cervi, V. Marc, and J.-P. Malet, "Field investigation of preferential fissure flow paths with hydrochemical analysis of small-scale sprinkling experiments," *Earth Surface Dynamics*, vol. 2, no. 1, pp. 181–195, Mar. 2014.
- [19] H. Rahardjo, T. T. Lee, E. C. Leong, and R. B. Rezaur, "Response of a residual soil slope to rainfall," *Canadian Geotechnical Journal*, vol. 42, no. 2, pp. 340–351, Apr. 2005.
- [20] P. Sitarénios, F. Casini, A. Askarinejad, and S. Springman, "Hydro-mechanical analysis of a surficial landslide triggered by artificial rainfall: the Ruedlingen field experiment," *Géotechnique*, vol. 71, no. 2, pp. 96–109, Feb. 2021.
- [21] P. Sun, H. Wang, G. Wang, R. Li, Z. Zhang, and X. Huo, "Field model experiments and numerical analysis of rainfall-induced shallow loess landslides," *Engineering Geology*, vol. 295, p. 106411, Dec. 2021.
- [22] M. Zhang, L. Yang, X. Ren, C. Zhang, T. Zhang, J. Zhang, and X. Shi, "Field model experiments to determine mechanisms of rainstorm-induced shallow landslides in the Feiyunjiang River basin, China," *Engineering Geology*, vol. 262, p. 105348, Nov. 2019.

- [23] F. Casini, V. Serri, and S. M. Springman, "Hydromechanical behaviour of a silty sand from a steep slope triggered by artificial rainfall: from unsaturated to saturated conditions," *Canadian Geotechnical Journal*, vol. 50, no. 1, pp. 28–40, Jan. 2013.
- [24] S. Cuomo, M. Moscarello, and V. Foresta, "Wetting tests of partially saturated soils under simple shear conditions," *Géotechnique Letters*, vol. 7, no. 2, pp. 197–203, Jun. 2017.
- [25] J. Peranić and v. Arbanas, "Impact of the wetting process on the hydro-mechanical behavior of unsaturated residual soil from flysch rock mass: preliminary results," *Bulletin of Engineering Geology and the Environment*, vol. 79, no. 2, pp. 985–998, Mar. 2020.
- [26] W. A. Take, M. D. Bolton, P. C. P. Wong, and F. J. Yeung, "Evaluation of landslide triggering mechanisms in model fill slopes," *Landslides*, vol. 1, no. 3, pp. 173–184, Sep. 2004.
- [27] A. Tohari, M. Nishigaki, and M. Komatsu, "Laboratory Rainfall-Induced Slope Failure with Moisture Content Measurement," *Journal of Geotechnical and Geoenvironmental Engineering*, vol. 133, no. 5, pp. 575–587, May 2007.
- [28] E. Damiano, R. Greco, A. Guida, L. Olivares, and L. Picarelli, "Investigation on rainwater infiltration into layered shallow covers in pyroclastic soils and its effect on slope stability," *Engineering Geology*, vol. 220, pp. 208–218, Mar. 2017.
- [29] G. Spolverino, G. Capparelli, and P. Versace, "An Instrumented Flume for Infiltration Process Modeling, Landslide Triggering and Propagation," *Geosciences*, vol. 9, no. 3, p. 108, Feb. 2019.
- [30] S. Pajalić, J. Peranić, S. Maksimović, N. Čeh, V. Jagodnik, and v. Arbanas, "Monitoring and Data Analysis in Small-Scale Landslide Physical Model," *Applied Sciences*, vol. 11, no. 11, p. 5040, May 2021.
- [31] K.-H. Yang, T. S. Nguyen, H. Rahardjo, and D.-G. Lin, "Deformation characteristics of unstable shallow slopes triggered by rainfall infiltration," *Bulletin of Engineering Geology and the Environment*, vol. 80, no. 1, pp. 317–344, Jan. 2021.
- [32] Ž. Arbanas, V. Jagodnik, J. Peranić, S. Pajalić, M. Vivoda Prodan, and N. Čeh, "Physical model of rainfall induced landslide in flume test: preliminary results," in *Proceedings of 4th European conference on physical modelling in geotechnics*. Lulea University of Technology, 2020.
- [33] V. Jagodnik, J. Peranić, and v. Arbanas, "Mechanism of Landslide Initiation in Small-Scale Sandy Slope Triggered by an Artificial Rain," in *Workshop on World Landslide Forum*. Springer, 2020, pp. 177–184.
- [34] R. S. Ladd, "Specimen Preparation and Liquefaction of Sands," *Journal of the Geotechnical Engineering Division*, vol. 100, no. 10, pp. 1180–1184, Oct. 1974.
- [35] A. Zanutta, P. Baldi, G. Bitelli, M. Cardinali, and A. V., "Qualitative and quantitative photogrammetric techniques for multi-temporal landslide analysis," *Annals of Geophysics*, vol. 49, no. 4-5, Dec. 2009.
- [36] T. Feng, H. Mi, M. Scaioni, G. Qiao, P. Lu, W. Wang, X. Tong, and R. Li, "Measurement of Surface Changes in a Scaled-Down Landslide Model Using High-Speed Stereo Image Sequences," *Photogrammetric Engineering & Remote Sensing*, vol. 82, no. 7, pp. 547–557, Jul. 2016.

- [37] G. Bitelli, M. Dubbini, and A. Zanutta, "Terrestrial laser scanning and digital photogrammetry techniques to monitor landslide bodies," *International Archives of Photogrammetry, Remote Sensing and Spatial Information Sciences*, vol. 35, no. B5, pp. 246–251, 2004.
- [38] G. C. Topp, J. L. Davis, and A. P. Annan, "Electromagnetic determination of soil water content: Measurements in coaxial transmission lines," *Water Resources Research*, vol. 16, no. 3, pp. 574–582, Jun. 1980.
- [39] "TEROS 10 Manual," accessed: 2022-03-01.
- [40] "TEROS 11/12 Manual," accessed: 2022-03-01.
- [41] "TEROS 21 Manual," accessed: 2022-03-01.
- [42] A. W. Bishop, "The principle of effective stress," *Teknisk ukeblad*, vol. 39, pp. 859–863, 1959.

Digital image correlation and the use of high-speed cameras for 3D displacement monitoring in 1g small-scale landslide models

Nina Čeh^{1*}, Josip Peranić¹, Vedran Jagodnik¹, Sara Pajalić¹, Martina Vivoda Prodan¹, and Željko Arbanas¹

¹University of Rijeka, Faculty of Civil Engineering, Rijeka, Radmile Matejčić 3, Croatia, +38551265943
*nina.ceh@gradri.uniri.h

Abstract

Small-scale physical models of landslides triggered by rainfall and seismic conditions provide a good insight into the initiation and progression of full-scale landslides in nature. In order to track and document the displacements on the surface of the small-scale model, a digital image correlation-based optical measuring system with high-speed cameras is used here. Each model is prepared for the optical measurements by adding specially chosen marker points (pins) that are monitored by a pair of high-speed cameras during each experiment. An additional set of non-high-speed cameras with higher resolution is used to monitor the deformation field on a selected smaller part of the model. This enables to obtain the 3D displacements and velocities of each marker point in order to detect any movement or crack opening on the surface both visually and accurately from the optical measurement results. The described system and established measurement procedure are advantageous as they provide the 3D displacement and velocity data for a large number of points on the surface with less equipment than conventional contact measurement methods. The collected data, in combination with other monitoring sensors, allow the observation of landslide initiation and the analysis of landslide evolution in all parts of the model slope during the sliding process. In this paper we present the measurement procedure and the results obtained optically in selected small-scale experiments.

Keywords: landslides, 1g small-scale models, digital image correlation, optical measurement, surface displacements.

1 Introduction

Landslides are one of world's major hazards with serious consequences for both infrastructure and human lives. Heavy and prolonged rainfall alone and in combination with dynamic events such as earthquakes increase landslide risk [1, 2]. Monitored and well-documented laboratory experiments conducted on small-scale landslide models allow for a better understanding of the conditions that influence and trigger landslide initiation, as well as the investigation of possible landslide mitigation measures. Motivated by this, a research project with an extensive experimental programme on small-scale landslide models was initiated, with an aim to investigate the behaviour of structures used for mitigation of landslides triggered in static or dynamic conditions. Static conditions imply rainfall, whereas dynamic conditions imply earthquake excitation (in combination with significant saturation of the soil in a slope) [2]. In order to monitor the displacement field at the slope surface in a small-scale landslide model, it is necessary to use an approach that does not

interfere with the model's geometry and the mass distribution on the slope. Non-contact optical measurement systems are chosen here, which can replace most of the conventional measurement devices for displacement and strain, as shown in [3–11].

2 Digital image correlation (DIC) and optical measuring system

A 3D optical measuring system comprises a set of two cameras connected to a control unit and a suitable software used to conduct the measurement as well as post-process the data [12, 13]. Here we use two optical measuring systems: GOM Aramis 4M and GOM Aramis 12M. Their characteristics are given in Tab. 1.

Table 1: Characteristics of the two Aramis optical measuring systems.

| System | Frame rate | Resolution (pixels) |
|------------|------------|--------------------------------------|
| Aramis 4M | 168 fps | 2400 x 1728 |
| | 1300 fps | 2400 x 168 |
| Aramis 12M | 25 fps | 4096 x 3000 pixels (full resolution) |
| | 75 fps | 4096 x 1000 pixels (1/3 of image) |
| | 100 fps | Reduced resolution (binning) |

The optical measuring procedure consists of calibration (with respect to the measuring volume or size of the monitored surface), surface preparation (which includes dyeing the whole surface or attaching marker points at discrete positions of interest, as shown in Fig. 1), measurement (obtaining pairs of snapshots at a given frequency throughout the experiment) and post-processing of the raw data. The results in the form of displacements of the surface points are obtained based on digital image correlation procedure in the post-processing, whereas the strains, velocities and any other values need to be derived from the displacements.



Figure 1: Pins with attached markers on the surface of the model.

3 Experimental set-up (experiment 14/02/2022)

The analysed experiment was conducted on a sandy slope with an angle of 35° exposed to a constant rainfall intensity of 73 mm/min [2, 14]. The optical measuring equipment is positioned as shown in Fig.

2 for all experiments with static conditions: the high-speed Aramis 4M system positioned to capture the entire surface of the model, and the high-resolution 12M system focused on a small part on the side of the model. The view from the left and right cameras of the 4M system is shown in Fig. 3, with the detected



Figure 2: Setup of the optical measuring system in models subjected to static loading conditions (simulated rainfall).

points marked in green. With a grid of 5 by 24 points, a total of 120 points were monitored. The experiment was optically monitored for 2 hours and 11 minutes, with a lower measurement frequency at the beginning, which was increased when surficial movements were detected (Tab. 2).

Table 2: The measuring frequency and duration of the optical measuring system.

| Part | Measuring frequency | dt | Duration |
|------|---------------------|-------|-----------------|
| 1 | 1/300 fps | 300 s | 52 min 59 s |
| 2 | 1/10 fps | 10 s | 1 h 18 min 11 s |

3.1 Results

The results are presented for the longitudinal profile shown in Fig. 4, which begins with point 2,1 in the lower part of the slope and ends with point 2,24 in the upper part of the slope. The position data of some markers are lost during the experiment due to water droplets accumulating on the markers and physical obstacles such as the elements of the sprinkler system or the reinforcements of the plexiglass side walls. Longitudinal profile 2 is chosen here for analysis, as all points (except point 2,1) were visible to both cameras. In addition to the profile considered, Fig. 4 shows the location of 2 points that are analysed in more detail due to their particular location in relation to the development of the landslide: points 2,19 and 2,21 near the upper part of the slope.

The orientation of the coordinate system used with the corresponding signs is given in Fig. 5. The shape of the profile throughout the experiment is shown in Fig. 6(top). There is clear evidence of the development of larger displacements in the top of the slope between stages 300 and 434, specifically between stages 390 and 434. These stages correspond to a test time of 121 and 128 minutes (or 7262 and 7702 seconds) after the start of the test, i.e. the rainfall simulation (see Fig. 6, bottom). Snapshots of stages 390 and 434 from the left camera are also shown in Fig. 13.

The behaviour of the points in the upper part of the slope in profile 2 is analysed in detail. The points at the top were not covered by water at any time during the rainfall simulation, so both cameras were able to take clear photos of them until the end of the experiment. The time courses of the vertical displacements



Figure 3: Left-camera (top) and right-camera (bottom) view of the model with monitored points (green dots) (from [2, 15]).



Figure 4: Longitudinal profile no. 2 in the reference stage and the location of the points used for the detailed analysis of the displacement evolution.

for the two chosen points (2,19 and 2,21) (marked in Fig. 4) are shown in Fig. 7. Fig. 7 shows that the vertical displacements of the monitored points in the upper part of the slope are close to zero until about 3700 seconds (which roughly corresponds to the time when the first instability at the very bottom of the slope is noticed), which is followed by a slow linear increase until the last part of the experiment, when a rapid non-linear increase occurs, announcing a failure of the slope. This can also be seen in Fig. 8, where the stage (i.e. time) corresponding to the significant increase in displacements and cracking at the top of the slope can be accurately identified.

A similar behaviour can be observed for the time courses of the horizontal displacements (Figs. ??

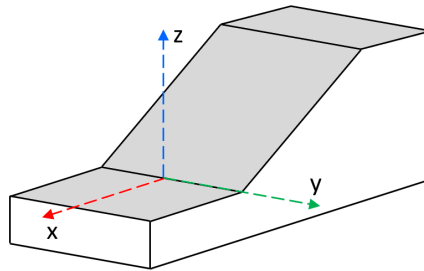


Figure 5: Coordinate system orientation used in the optical measurement and post-processing.

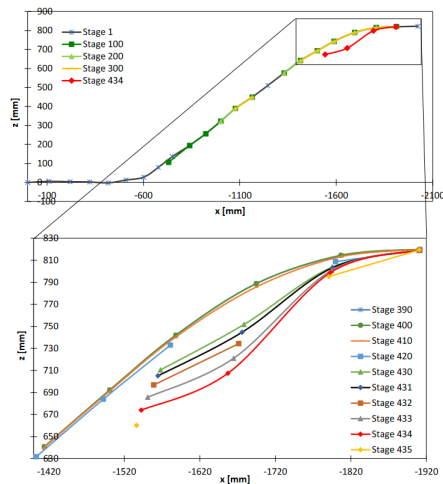


Figure 6: Longitudinal profile no. 2 shown in the x-y plane throughout the experiment (top) and the upper part of the profile between stage 390 and 435 (bottom) [2, 15].

and ??). The two horizontal directions are defined so that the x-direction is longitudinal and the y-direction is transverse (see Fig. 5). Positive and negative values in the y-direction mean a movement down and up the slope, respectively, while positive and negative values in the x-direction mean a movement to the right and to the left, respectively, as seen from the crown.

We can again notice a slow linear increase between 3700 and 7500 seconds and a significant non-linear increase after that in x direction displacements, while y direction displacements increase as well, but the displacements are lower. Both directions are better analysed in Figs. 11 and 12, where the time when the displacements start to increase in a non-linear manner can be determined more precisely.

A series of nine snapshots taken by the left camera during the last part of the experiment is shown in Fig. 12.

An increase in the vertical displacements of points 2,19 and 2,21 in Figs. 6-11 can be seen after $t=7400$ s. However, as can be seen from stage 420 ($t=7562$ s) in Fig. 12, it is difficult to see only by visual inspection of the scaled slope model, that the points experience significant movements in the period before they are affected by the retrogressive sliding, as can be clearly seen for stage 430 ($t=7662$ s) in the same figure.

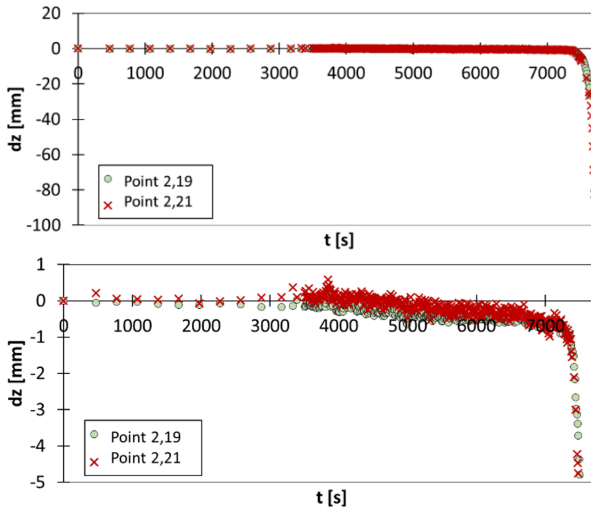


Figure 7: Time course of the displacements along the z-axis of points 2,19 and 2,21 in the upper part of the scaled slope: displacements on a scale up to -100 mm (top) and up to -5 mm (bottom)

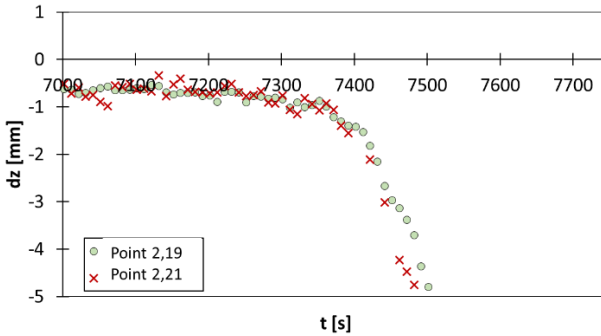


Figure 8: Time course of the displacements along the z-axis of points 2,19 and 2,21 between 116 and 130 minutes in the experiment (7000 and 7800 seconds, respectively).

The rapid increase in vertical displacements in Fig. 7 corresponds to the progression of instability in the form of the retrogressive sliding towards the top of the slope. As given in Tab. 2 the optical measurements are obtained from snapshots taken every 10 seconds in this part of the experiment, which results in 10 snapshots between the two stages of interest: stage 420 and 430. The used optical system, however, is able to monitor the model with frequency up to 168 fps, but limited to less than 60 seconds of continuous monitoring due to RAM capacity of the system. It is important to note that the time from the first instability in the model, which took the form of a small rotational slide at the foot of the slope due to groundwater level rise, to when the retrogressive slide reached the analysed points at the top of the slope was about 60 minutes. Thus, monitoring the entire instability evolution with high frequency is not possible. These observations suggest that in the case where high frequency data of surface displacements are needed, i.e.

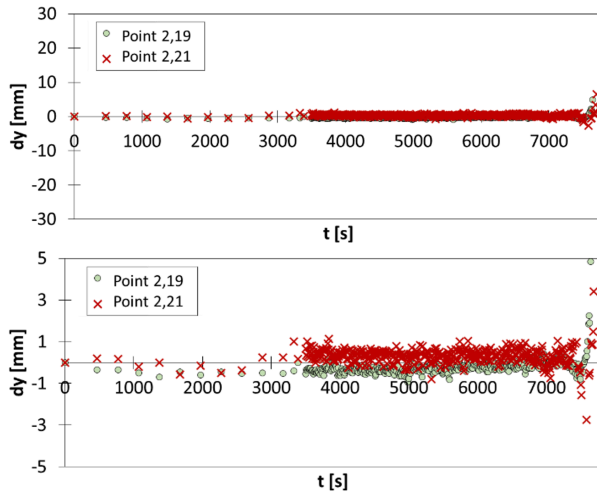


Figure 9: Time course of the displacements along the y-axis of points 2,19 and 2,21 in the upper part of the scaled slope: displacements on a scale up to -30 mm (top) and up to -5 mm (bottom)

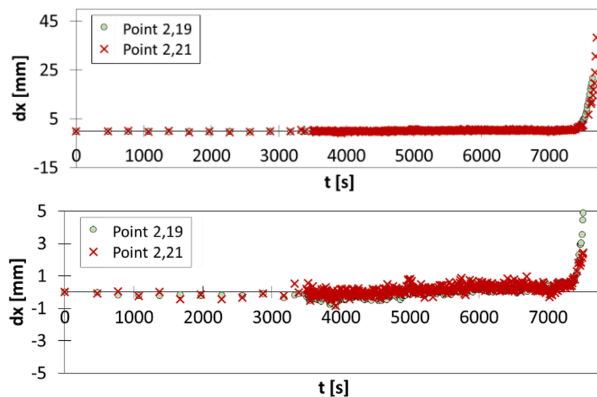


Figure 10: Time course of the displacements along the x-axis of points 2,19 and 2,21 in the upper part of the scaled slope: displacements on a scale from -15 to 45 mm (top) and from -5 to 5 mm (bottom)

in the analysis of processes that develop relatively quickly after a long period of inactivity, as is the case with fast moving flow-like landslides, rockfalls and tracking of the rockfall trajectories and/or the impact forces and interaction of fast moving slope material with the landslide remediation structures in scaled slope models etc., the usefulness of the non-contact measurement system, as the one presented in this study, becomes limited due to the requirement of postprocessing of the measurement data. However, the data obtained concurrently with some of the conventional monitoring techniques (geodetic and/or geotechnical) that allow real-time monitoring of displacements or other quantities that can be used as indications that the scaled slope is approaching conditions of instability could be used to adjust the frequency of data collection and optimise the monitoring process of such non-contact systems during all phases of instability development,

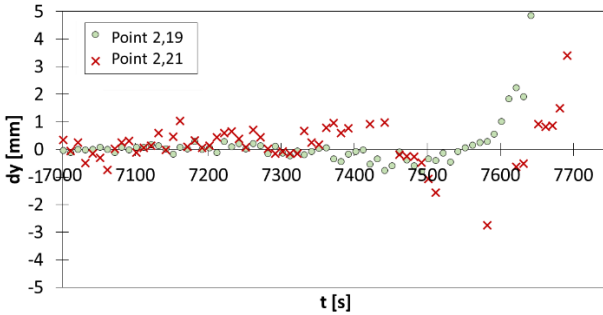


Figure 11: Time course of the displacements along the y-axis of points 2,19 and 2,21 in the upper part of the scaled slope.

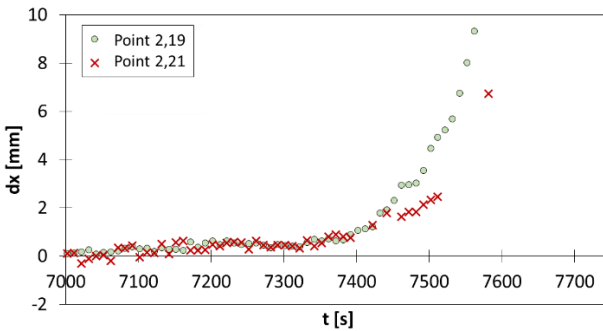


Figure 12: Time course of the displacements along the x-axis of points 2,19 and 2,21 in the upper part of the scaled slope.

i.e. from stable conditions through the phase of initiation of movement to deposition at the end. This could be the approach that would provide adequate data for a detailed analysis of the instability process and the mechanisms involved.

4 Discussion and Conclusions

Displacement data obtained with an optical measurement technique from an experiment conducted on a small-scale sandy slope initiated by simulated rainfall are presented. Two non-contact optical measurement systems, a high-speed camera system and a slower system with higher resolution, are used to monitor the 3D displacements of the surface of the model. Based on sets of snapshots from two precisely tuned cameras, the displacements of the marker points on the slope are obtained, post-processed and analysed. A longitudinal profile of interest is presented here, where we can easily keep track of the profile shape throughout the experiment. Furthermore, the displacement data of two selected points at the top of the slope, combined with a series of snapshots, show how a significant increase in displacement can be detected and used to accurately detect any instability or cracking. Such an optical measurement method using high-speed camera systems in combination with other monitoring sensors installed in the model can provide much important and well-documented data describing the behaviour of the surface in a small-scale landslide test.

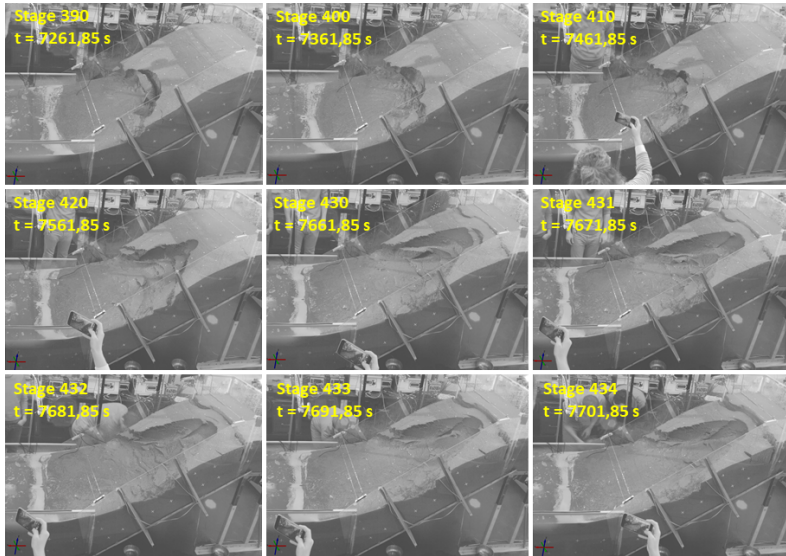


Figure 13: Left camera snapshots on the stages shown in Fig. 4 (corresponding to time between 7261.85 s in stage 390 and 7261.85 s in stage 434).

Acknowledgements

This work is supported by Croatian Science Foundation under the Project IP-2018-01-1503 Physical modelling of landslide remediation constructions behaviour under static and seismic actions (ModLandRemSS).

References

- [1] D. Petley, "Global patterns of loss of life from landslides," *Geology*, vol. 40, no. 10, pp. 927–930, oct 2012.
- [2] S. Pajalić, J. Peranić, S. Maksimović, N. Čeh, V. Jagodnik, and Ž. Arbanas, "Monitoring and Data Analysis in Small-Scale Landslide Physical Model," *Applied Sciences*, vol. 11, no. 11, p. 5040, may 2021.
- [3] O. Hunger and N. R. Morgenstern, "Experiments on the flow behaviour of granular materials at high velocity in an open channel," *Géotechnique*, vol. 34, no. 3, pp. 405–413, sep 1984.
- [4] Y. Okura, H. Kitahara, H. Ochiai, T. Sammori, and A. Kawanami, "Landslide fluidization process by flume experiments," *Engineering Geology*, vol. 66, no. 1-2, pp. 65–78, oct 2002.
- [5] H. Moriwaki, T. Inokuchi, T. Hattarji, K. Sassa, H. Ochiai, and G. Wang, "Failure processes in a full-scale landslide experiment using a rainfall simulator," *Landslides*, vol. 4, no. 1, pp. 277–288, 2004.
- [6] R. P. Orense, S. Shimoma, K. Maeda, and I. Towhata, "Instrumented Model Slope Failure due to Water Seepage," *Journal of Natural Disaster Science*, vol. 26, no. 1, pp. 15–26, 2004.

- [7] L. D. Suits, T. C. Sheahan, L. Olivares, E. Damiano, R. Greco, L. Zeni, L. Picarelli, A. Minardo, A. Guida, and R. Bernini, "An Instrumented Flume to Investigate the Mechanics of Rainfall-Induced Landslides in Unsaturated Granular Soils," *Geotechnical Testing Journal*, vol. 32, no. 2, p. 101366, 2009.
- [8] M. Scaioni, P. Lu, T. Feng, W. Chen, G. Qiao, H. Wu, X. Tong, W. Wang, & R. Li, and R. Li, "Analysis of spatial sensor network observations during landslide simulation experiments," *European Journal of Environmental and Civil Engineering*, vol. 17, pp. 802–825, 2013.
- [9] G. L. Ooi, Y. H. Wang, P. S. Tan, C. F. So, M. L. Leung, X. Li, and K. H. Lok, "An instrumented flume to characterize the initiation features of flow landslides," *Geotechnical Testing Journal*, vol. 37, no. 5, sep 2014.
- [10] P. Lu, H. Wu, G. Qiao, W. Li, M. Scaioni, T. Feng, S. Liu, W. Chen, N. Li, C. Liu, X. Tong, Y. Hong, and R. Li, "Model test study on monitoring dynamic process of slope failure through spatial sensor network," *Environmental Earth Sciences*, vol. 74, no. 4, pp. 3315–3332, aug 2015.
- [11] T. Feng, H. Mi, M. Scaioni, G. Qiao, P. Lu, W. Wang, X. Tong, and R. Li, "Measurement of Surface Changes in a Scaled-Down Landslide Model Using High-Speed Stereo Image Sequences," *Photogrammetric Engineering & Remote Sensing*, vol. 82, no. 7, pp. 547–557, 2016.
- [12] S. Dobrilla, N. Čeh, M. Tuhtan, and G. Jelenić, "Eksperimentalna analiza odziva grednog nosača na nejednoliku pobudu oslonaca Experimental Analysis of Structure Response to Non-uniform Support Excitation," *Zbornik radova*, vol. 20, no. 1, pp. 175–188, jul 2018.
- [13] N. Čeh, G. Jelenić, and N. Bičanić, "Analysis of restitution in rocking of single rigid blocks," *Acta Mechanica*, vol. 229, no. 11, pp. 4623–4642, nov 2018.
- [14] Ž. Arbanas, V. Jagodnik, J. Peranić, S. Pajalić, M. Vivoda Prodan, and N. Čeh, "Physical model of rainfall induced landslide in flume test: preliminary results," in *Proceedings of 4th European conference on physical modelling in geotechnics. Lulea University of Technology*, 2020.
- [15] S. Maksimović, "Analiza površinskih pomaka na modelu klizišta," Ph.D. dissertation, University of Rijeka, Faculty of Civil Engineering, Rijeka, sep 2020.

Physical modelling investigation and integrated analysis of landslides for defining risk scenarios

Giovanna Capparelli^{1,*}, Gennaro Spolverino¹, Irasema Alcántara-Ayala², and Noemi Sharon Ruiz-Cortés²

¹ *Università della Calabria, Dipartimento di Ingegneria Informatica, Modellistica, Elettronica e Sistemistica, Arcavacata di Rende (CS), via P. Bucci, Italy. +39 3475446857*

² *National Autonomous University of Mexico (UNAM), Institute of Geography, Mexico City, Mexico. *giovanna.capparelli@unical.it*

Abstract

Predicting natural processes, such as rainfall-induced landslides, is a problem of great importance. Every year, meteorological events trigger both superficial and deep landslides on many slopes, causing damage and victims. The study presented here focuses on the hydraulic and hydrologic issues that take place in an unstable slope under the rainfall infiltration. The mentioned studies are dealt through a physical modelling, a numerical simulation techniques, and through in situ experimental measurements. Our research is based on an integrated approach which, starting from the observation of the real phenomenon, reproduces the observed phenomenon in the laboratory and models it using an appropriate mathematical scheme. The in situ data refer to a monitoring station installed near the site where a large mudflow occurred. The physical model consists of 2 connected, independently tilting flume branches (respectively designed to study landslide triggering and propagation), each 1m wide and 3m long. The flume is equipped with tensiometers for measuring soil water potential inside the slope, a Time Domain Reflectometry (TDR) system and probes for measuring soil volumetric water content, and laser transducers for measuring soil surface displacements in the direction orthogonal to the sliding plane. The analysed landslide-prone area is located in Campania (southern Italy), where disastrous mudflows occurred in May 1998, with many human casualties. The applications allow a better understanding of the role of the rainfall infiltration and pore water pressure changes in the triggering mechanism, and suggests how the porosity of the soils involved can affect the kinematic behaviour. The author believes that these changes must be carefully considered when assessing hazard levels, planning mitigation interventions regarding slope stability and designing future mitigation strategies for risk reduction.

Keywords: Laboratory flume tests, triggering model, hazard assessment

1 Experimental Site

Catastrophic mudflows often occur in mountains covered with volcanic soils. Some examples of these landslides are those that occurred in southern Italy, near the volcano Vesuvius and those that occurred in Mexico. In fact, significant rainfall-induced landslides have taken place in Mexico. In particular, in the Sierra Norte de Puebla, a mountain system in the state of Puebla within the transition of the physiographic provinces the Sierra Madre Oriental and the Trans-Mexican Volcanic Belt, these phenomena are recurrent [1, 2]. Such recurrence derives from the physical characteristics of the territory, characterized by its exposure to hydro-meteorological events including tropical storms and hurricanes, but also due to the presence of mountain ranges with steep slopes and complex geology composed by sedimentary and metamorphic

rocks overlaid by volcanic material such as ignimbrite and ash-pumice flow deposits [2, 3] resulted from the activity of the Los Humeros caldera [4]. Owing to the vulnerability conditions of people living in these areas, disasters triggered by rainfall-induced landslides are frequent in this region [5]. The worst and latest episode took place in October 1999 in the municipality of Teziutlán. This municipality is located on a large plateau extent of a non-welded pyroclastic deposit of ignimbrite type, characterized by a sandy texture and the presence of pumice fragments. In 1999, extraordinarily heavy rains associated with Tropical Depression *N°11* in the Gulf of Mexico triggered a large number of landslides leading to the largest disaster in decades, with significant human and economic losses, including 263 fatalities [2, 5, 6]. The instability of pyroclastic soils is one of the most topical and catastrophic problems involving also the Campania region (southern Italy). In this area, several volcanic eruptions of large complexes, i.e. Somma-Vesuvius, Campi Flegrei and Roccamonfina, have occurred over the last 40,000 years [7, 8]. The resulting materials are spread over a large area around the City of Naples and the slope coverings are frequently affected by to rain-induced landslides. (e.g. [9–11]). In recent years, the scientific community has been urged to study and investigate the instability of soils of pyroclastic origin covering the slopes around the Vesuvius area (Naples, Italy). In particular the Pizzo d'Alvano ridge has been analyzed, especially following the tragic landslide events of 5-6 May 1998 which killed 152 people. In this area the deposits are incoherent, varying in grain size from sands, silty sands and silts (ashes) to gravels and sands with gravels (pumices). In particular, the ashes show a rather variable degree of compaction, with porosity ranging from 0.5 to 0.75 [12]. Along the slopes, the hydrogeological characteristics of the pyroclastic deposits are mainly related to the continuity of the ash and pumice layers, which affect the rainfall infiltration process. In the area described, the decision was made to install a monitoring station to study the infiltration processes responsible for triggering landslides. The station was installed in particular geological-stratigraphic and geomorphologic conditions. Specifically, the monitored site is located in the upper part of the slope of Pizzo d'Alvano, near the relief known as "Torre Savaio" and close to some of the landslides that occurred in Sarno in May 1998. This site is of particular interest because it represents an area that was not affected by the landslide events of May 1998 at Sarno and it represents, with good approximation, the pre-event hydrogeological conditions.

1.1 Monitoring Station

The monitoring station consists of 7 tensiometers and 8 Time Domain Reflectometry (TDR) probes at different depths to measure suction (ψ) and volumetric water content (Θ), respectively. The sensors continuously record the state of the soil, taking systematic measurements every minute. The data is sent to a data logger at 10-minute intervals and can be downloaded directly on site or from a remote server. In addition to the sensors monitoring the ground conditions, a tipping rain gauge was installed to record rainfall events at the site. The station uses electricity from a battery which is recharged by a solar panel. The installation of the station was preceded by the construction of a hand-dug trench, approximately 2m wide and 2m deep. The TDR probes were pushed horizontally into the walls of the trench at various depths (depths indicated in Fig. 2). At the points where they emerged from the ground, the sensors were protected by concrete manholes.

The cables were routed through a spiral pipe, which in turn was protected by a double-walled cable duct. The schematic of the monitoring station is shown in Figure 1. Direct investigations carried out on site (exploratory pits and trenches) delineated the stratigraphy and thickness of the pyroclastic blanket, revealing the alternation of sandy-gravelly pumices interspersed with silt-sandy-clay cineritic palaeosols. The stratigraphy and the levels affected by the installation of the sensors are shown schematically in Figure 2.

The data recorded by the monitoring station for the hydrological year from 01.10.2015. to 30.09.2016. were analysed and an initial screening was performed, eliminating all "no-data" readings and all unreliable figures. Pairs of suction and water content measurements recorded at the same time at the same depths were correlated in order to construct the soil water retention curve. These values were interpolated with the mathematical formulation of the van Genuchten model curve [13]. Figure 3 shows the pairs of suction

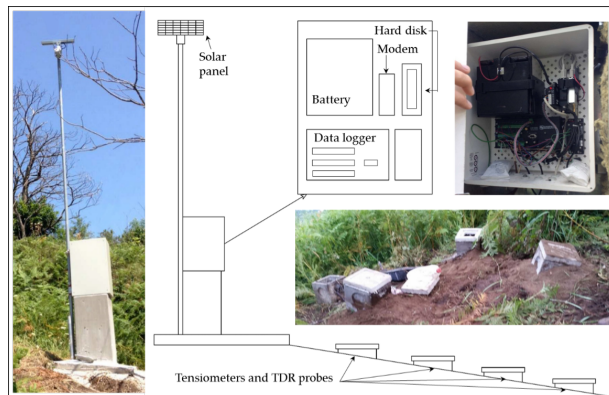


Figure 1: Monitoring station diagram.

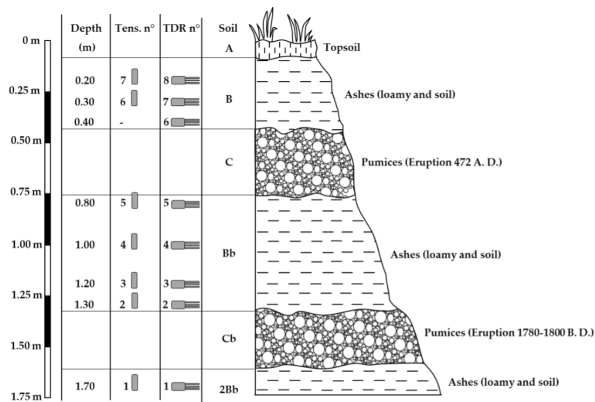


Figure 2: Stratigraphy and the levels affected by the installation of the sensors.

and saturation degree values and the curve identified by their interpolation. The graph also shows the main imbibition and drying curves obtained from a laboratory test [14].

The curve obtained by interpolating the on-site data lies within the hysteresis formed by the two main curves. This was to be expected, since the data used to construct the curve refer to both periods of infiltration and drying. The result is therefore, an average water retention curve that takes into account both imbibition and drying processes.

2 Physical model

The physical model is a channel with a rectangular cross-section that is homogeneous and constant along its entire length [15]. The structure, supported by metal pipes, is 1 m high, 6 m long in total, divided into 3 m for the triggering and 3 m for the propagation, and 1 m wide. Figure 4 shows the side and front views of the channel. Both the side walls and the bottom wall are made of transparent plexiglass panels to ensure

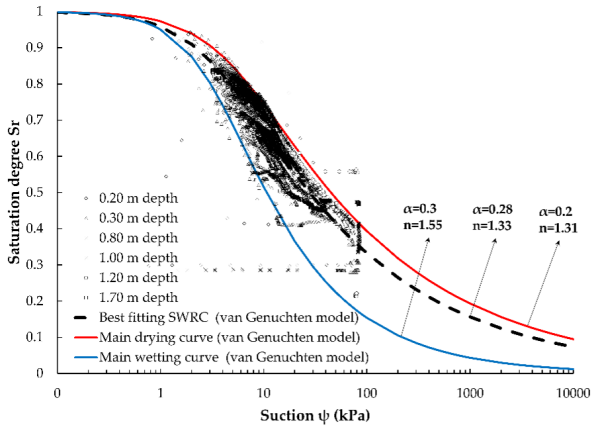


Figure 3: Pairs of suction and saturation degree values, the curve identified by their interpolation, and the main imbibition and drying curves obtained from a laboratory test.

that the movement can be both viewed and filmed during the landslide. On the flume bed it is possible to reproduce both an impermeable and permeable bottom-base. In the former case, an impermeable rough bed is laid, which acts as an interface with the test soil, consisting of a plastic sheet on which gravel grains are glued; in the latter case, a permeable geotextile or geonet is used. To hold the deposit, a draining grid is laid at the foot of the reconstructed slope.

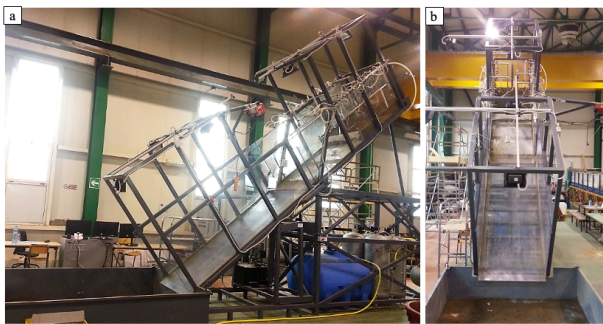


Figure 4: Physical model: (a) side view; and (b) frontal view.

Grids of different heights can be inserted according to the thickness of the reconstructed deposit. The grid is formed by a perforated metal sheet, on which a permeable geotextile is placed which permits drainage. Moreover, on the front part of the grid, transversal to the slope, small water collection channels can be mounted to measure both surface runoff and runoff from the individual soil layers. Artificial rainfall was applied with a 24-nozzle water particle sprinkler system, fed by a main 1000-liter tank and four 200-liter auxiliary tanks. The rainfall system integrates four pressure sensors and three auxiliary rain gauges. The arrangement of the nozzles was optimized so as to ensure rainfall uniformity, and minimize surface erosion and interference with the video system. The pressure range varies between 0.1 and 7 bar with an intensity that can vary according to the nozzles used. The maximum variation, for each nozzle, ranges from 0.28

to 6.13 mm/h. In addition to the artificial rainfall system, further acquisition systems are installed which permit data collection with a series of sensors for a total of 48 channels from tensiometers, pressure transducer, laser sensors to detect the soil level, auxiliary sensors (inclination and pressure) and rain gauges. The individual sensors are placed in various positions and each may be positioned to operate on various measurement configurations and simulations. Finally, a series of motorized activation and control systems were installed, including pneumatic and hydraulic controls. The instrumentation in the artificial channel is able to measure the main parameters that control the physical phenomenon, thanks to the installation of the following equipment:

- Tensiometers (used to measure soil suction);
- Pressure transducers (used to measure pore water pressure);
- TDR device (used to measure soil water content);
- Rainfall system (used to simulate rainfall);
- Laser sensors (used to measure the soil profile and uz displacements);
- High-resolution video cameras (used to measure displacements along u_x and u_y).

This sensor system is essential for measuring and monitoring the main parameters that control and regulate the phenomenon of landslides triggered by rainfall infiltration.

2.1 First test with homogeneous soil

The pyroclastic soil used for the experimental tests was collected in the area of Sarno in southern Italy, about 15 km from the volcano Vesuvius. In May 1998, in this area, large and rapid landslides devastated the town, causing an enormous number of victims. At these sites, the stratigraphy consists of limestones covered by layers of pyroclastic deposits. These soils are the product of different eruptions of more volcanoes like Somma-Vesuvius, Flegrei fields and other volcanoes present in the region that are no longer active. The ashes, coming out after the eruption and carried by the wind, travel for kilometres from the eruption zone, resulting in a non-uniform stratigraphy throughout the region ([9, 16, 17]). Generally, they are incoherent deposits with variable granulometry, ranging from sands, silty sands and silts (ashes) to sands with gravel (pumice) and gravels. Inside the flume test, a homogeneous deposit of pyroclastic ash has been reconstructed, which can be attributed to the Plinian eruption of "Pollena" of 472 B.C. The slope was formed by a layer of volcanic ash 20 cm thick, occupied the entire width of the flume (100 cm) and was 150 cm long. This geometry allows the deposit to be assimilated to an indefinite slope. At the base of the model there was an impervious rough bed to simulate conditions similar to those of a natural slope. At the foot of the slope a geotextile-coated drainage grid was placed. The ash in question was sieved with a 0.4 cm mesh to remove coarse contamination occurring during the sampling phase. The artificial slope was re-constituted inside the flume by layers with the moist-tamping technique, with volcanic ash porosity of between 68% and 76%. The volumetric water content of the ash (Θ) was about 20%. Inside the artificial slope, 12 tensiometers were installed to measure suction and six TDR probes to measure volumetric water content. The sensors were installed at depths of 5 cm, 11 cm and 17 cm below the ground surface, both in the upslope and downslope zones of the deposit. Three neutral pressure transducers were arranged on the flume bed, while four laser displacement transducers were installed to measure displacements perpendicular to the slope surface. Figure 5 shows schematically the location of the sensors installed inside the deposit. Rainfall was generated by a sprinkler system placed about 100 cm above the sliding surface. The nozzles were arranged so as to ensure rainfall uniformity and avoid surface erosion. Several test stages were carried out:

1. The first test was conducted with the deposit in a horizontal position. A constant rainfall of considerable intensity was simulated (about 220 mm/h) for about 50 minutes. The test was performed to activate infiltration phenomena so as to stabilize the slope before tilting.
2. The deposit was then left under natural evaporation for about 14 days, acquiring the values recorded by the various sensors.
3. The slope was then inclined at 38° and exposed to evaporation for about 8 days to redistribute the suction values and water content in the new configuration.
4. Finally, a new infiltration phase was simulated with constant rainfall at an intensity of about 220 mm/h, which lasted until slope failure (about 40 minutes).

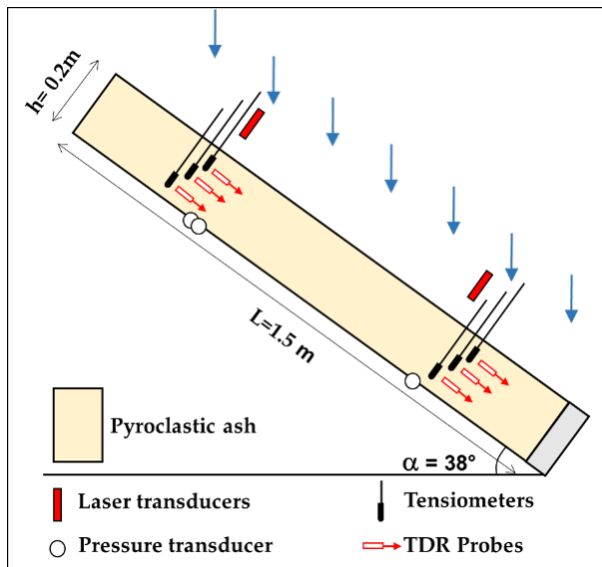


Figure 5: Position of the sensors in section in test n.1.

2.2 Test results

During the various tests, values of suction and volumetric water content were acquired both in the upslope and downslope zones at different depths. Displacements perpendicular to the slope surface were also measured, produced by the variation in the tension state, and the water pressure on the flume bed. The final infiltration phase was initiated with inclined deposit, with a high-intensity artificial rainfall (about 220 mm/h) to reach conditions that trigger a landslide along the artificial slope. The suction pattern during the last infiltration phase (Figure 6) clearly shows that saturation conditions at many of the tensiometers are swiftly reached. It is also possible to note the moment in which the curves for tensiometers placed downslope at 5 cm and 11 cm of depth have a rapid variation in slope, that is when part of the slope is detached and a small surface landslide is triggered. Trends in soil volumetric water content are reported in Figure 7. It appears evident, also in this phase of infiltration in a sloping channel, the progressive advancement of a wetting front from the top, although some differences are observed between the upslope and downslope

zones where, perhaps due to the imperfect homogeneity of the spatial distribution of the artificial rainfall, but especially due to the subsurface flow parallel to the slope, the increase in water content appears anticipated. It should also be pointed out that all the TDR probes, despite there being absolute evidence that much of the deposit reaches complete saturation conditions, detected water content values between 50% and 55%. This is doubtless to be attributed to compaction experienced by the deposit during the previous test phases, which had led to a reduction in height from the initial 20 cm to around 18 cm, corresponding to an estimated reduction in porosity of around 10%. This graph also shows the moment in which a small landslide is detached, producing an abrupt change in the steepness of the curve for the TDR positioned in the most superficial part downslope. In this case the landslide brought the TDR to the surface and from this point on, the values measured by the sensor are no longer representative of the actual water content.

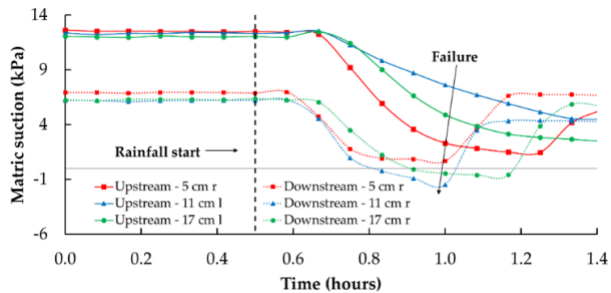


Figure 6: Time course of suction.

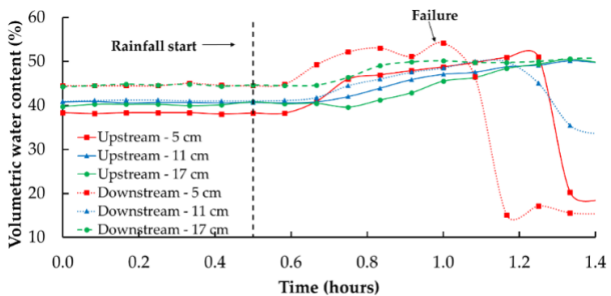


Figure 7: Volumetric water content vs. time.

Slope failure, consistent with the compacted configuration assumed by the deposit during the previous test phases, did not trigger a mud-flow. The instability took the form of a progressive erosion of the more superficial soil layers, initially and chiefly concentrated in the downslope zone, where the intense subsurface flow resulted in conditions of greater moisture being reached and, at the same time, encouraged soil mobilization. The first local failures began to occur about 20 minutes after the beginning of artificial rainfall, and only after that did they extend so far as to affect the points in which some of the tensiometers and TDR probes had been installed.

2.3 Second test with homogeneous soil

A homogeneous deposit of volcanic ash was reconstructed, similar to that of the previous test: 20 cm thick, 60 cm wide and 270 cm long (Figure 8). Also in this case, an impervious rough bed was placed, while a geotextile-coated drainage was placed at the foot of the slope. The porosity was between 68% and 76% and the volumetric water content of the ashes was about 20%. Inside the deposit, 12 tensiometers were installed to measure the suction, and 7 TDR probes to measure the volumetric water content. At the bottom of the flume, 6 pressure transducers were arranged, while 6 laser technology displacement transducers were installed to measure the displacements orthogonal to its surface of the slope. Figure 8 shows the position of the sensors in section. Rainfall was generated by a sprinkler system placed about 100 cm above the sliding surface. The nozzles were arranged so as to ensure rainfall uniformity and avoid surface erosion.

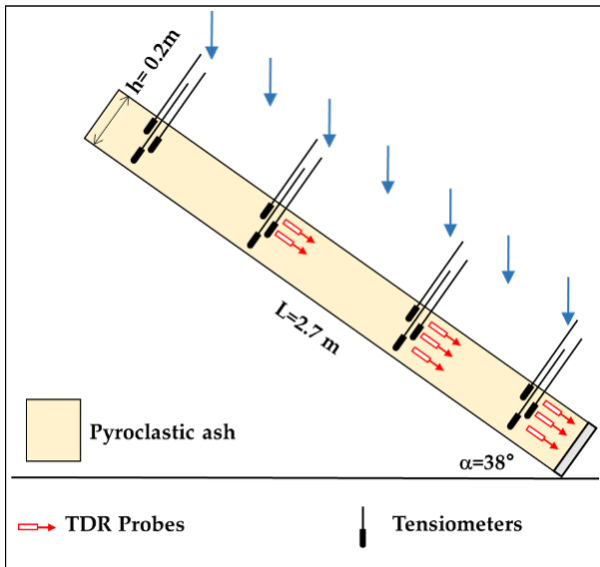


Figure 8: Position of the sensors in section in test n.2.

Various test stages were carried out:

1. The first phase was performed with the deposit in a horizontal position simulating a constant rain of 50 mm/h intensity for about 20 minutes, to activate infiltration phenomena so as to stabilize the slope before tilting it.
2. Subsequently, the slope was inclined at 38° and left to evaporate for about 20 days, in order to redistribute the suction and water content values in the new configuration.
3. Finally, an infiltration phase was carried out, simulating a rainfall with a constant intensity of 50 mm/h, which lasted about 4 hours, until the slope failure.

2.4 Test results

The last infiltration phase with the inclined deposit was characterized by artificial rainfall with an intensity of 50 mm/h. The evolution of suction during this phase until the slope failure is represented in Figure 9. This shows that all the values recorded by the tensiometers tend to converge to a suction value equal to zero, which indicates the achievement of the saturation condition in the entire deposit. The values of the volumetric water content were measured with 7 TDR probes. The trends are shown in Figure 10 from which note the progressive advancement of the wet front from top to bottom. Differences can be observed between the upstream and downstream areas, presumably due to an imperfect homogeneity of the spatial distribution of rainfall, but above all due to the sub-surface flow parallel to the slope. From the graph it can be seen that failure phenomena occurred about 120-130 minutes from the start of the test. There was a detachment of a large area of the soil which caused the triggering of an evident mudflow (Figure 11). In this test, in contrast to the first, there was a sudden detachment of the soil and the formation of a mudslide. This difference in behavior is due to the greater porosity of the soil in the second test.

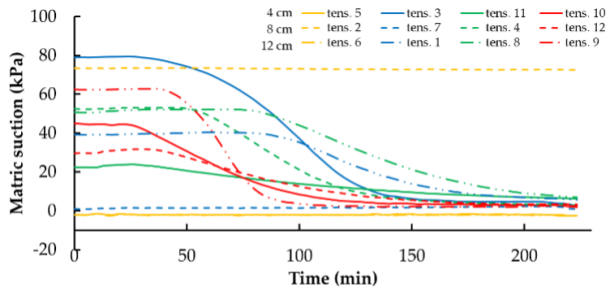


Figure 9: Time course of suction.

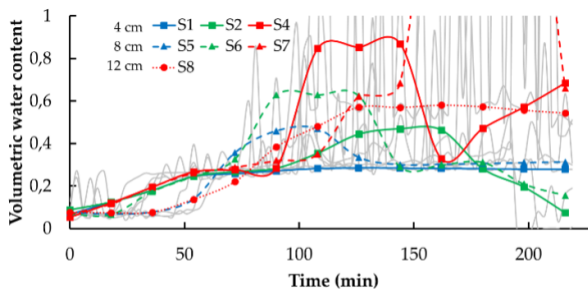


Figure 10: Volumetric water content vs. time.

This avoided the formation of volumetric collapse and therefore of soil compaction. We can therefore deduce that these soils lead to the formation of mudslides only if they maintain a high porosity, otherwise the detachments will be minor and retrogressive in nature.



Figure 11: Detachment niche of the mudflow.

3 Conclusions

In this work, experimental data on site were presented, measured by a monitoring station installed in Sarno, in southern Italy. This area was affected by several mudflows in May 1998, causing a lot of damage and deaths. The suction values and saturation degrees recorded at different depths for an entire hydrological year were analyzed. Pairs of values of these quantities made it possible to define the water retention curves. It has been shown that the SWRC of these soils show a strong hysteresis between the wetting and drying phases. This aspect must be taken into consideration when performing numerical simulations aimed at defining the mechanical response of the slope. Two experimental tests performed with a physical laboratory slope model were also presented. In both cases, the deposits were homogeneous and composed of pyroclastic ashes. Tests were developed in different test stages: phases of rainfall infiltration and evaporation with horizontal deposit, and rainfall phases with the deposit inclined. The mechanical response of the deposits in the two tests was decidedly different. In the first test, the instability occurred in a form of small detachments of a retrogressive nature. In the second, however, there was a mudflow. This difference is due to the different porosity of the soil. In fact, in the second test, the rainfall and evaporation phases with the horizontal deposit lasted much shorter than in the first test. This avoided the phenomenon of volumetric collapse and thus the compaction of the soil. This experimentation is grounds for the study of pyroclastic soil samples from other areas such as Sierra Norte de Puebla in Mexico, with the aim of highlighting any similarities in behavior and response to rainfall infiltration.

Acknowledgements

The authors gratefully acknowledge the financial support provided by the framework of the "SILA – PON_{a3_00341}" project An Integrated System of Laboratories for the Environment.

References

- [1] P. Flores Lorenzo and I. Alcántara Ayala, "Cartografía morfogenética e identificación de procesos de ladera en Teziutlan, Puebla," *Investigaciones geográficas*, pp. 7 – 26, Dec. 2002, publisher: scielomx.
- [2] I. Alcántara-Ayala, "Hazard assessment of rainfall-induced landsliding in Mexico," *Geomorphology*, vol. 61, no. 1-2, pp. 19–40, Jul. 2004.
- [3] F. G. Murillo-García and I. Alcántara-Ayala, "Landslide inventory, Teziutlán municipality, Puebla, México (1942–2015)," *Journal of Maps*, vol. 13, no. 2, pp. 767–776, Nov. 2017.
- [4] H. Ferriz and G. A. Mahood, "Eruption rates and compositional trends at Los Humeros Volcanic Center, Puebla, Mexico," *Journal of Geophysical Research*, vol. 89, no. B10, p. 8511, 1984.
- [5] I. Alcántara Ayala, R. J. Garnica Peña, A. Coll-Hurtado, and M. T. Gutiérrez Vázquez de MacGregor, "Inestabilidad de laderas en Teziutlán, Puebla," Tech. Rep., 2017, publisher: Universidad Nacional Autónoma de México.
- [6] D. B. Bitran, *Evaluación del impacto socioeconómico de los principales desastres naturales ocurridos en la República Mexicana, durante 1999 (Evaluation of the socioeconomic impact of the main natural disasters that occurred in the Mexican Republic during 1999)*. Mexico (In Spanish): Centro Nacional de Prevención de Desastres, 2000.
- [7] G. Rolandi, F. Bellucci, M. T. Heizler, H. E. Belkin, and B. De Vivo, "Tectonic controls on the genesis of ignimbrites from the Campanian Volcanic Zone, southern Italy," *Mineralogy and Petrology*, vol. 79, no. 1-2, pp. 3–31, Oct. 2003.
- [8] G. Di Crescenzo and A. Santo, "Debris slides—rapid earth flows in the carbonate massifs of the Campania region (Southern Italy): morphological and morphometric data for evaluating triggering susceptibility," *Geomorphology*, vol. 66, no. 1-4, pp. 255–276, Mar. 2005.
- [9] L. Cascini, S. Cuomo, and D. Guida, "Typical source areas of May 1998 flow-like mass movements in the Campania region, Southern Italy," *Engineering Geology*, vol. 96, no. 3-4, pp. 107–125, Feb. 2008.
- [10] P. Revellino, F. M. Guadagno, and O. Hungr, "Morphological methods and dynamic modelling in landslide hazard assessment of the Campania Apennine carbonate slope," *Landslides*, vol. 5, no. 1, pp. 59–70, Feb. 2008.
- [11] D. Di Martire, M. De Rosa, V. Pesce, M. A. Santangelo, and D. Calcaterra, "Landslide hazard and land management in high-density urban areas of Campania region, Italy," *Natural Hazards and Earth System Sciences*, vol. 12, no. 4, pp. 905–926, Apr. 2012.
- [12] G. Sorbino and M. V. Nicotera, "Unsaturated soil mechanics in rainfall-induced flow landslides," *Engineering Geology*, vol. 165, pp. 105–132, Oct. 2013.
- [13] M. T. van Genuchten, "A Closed-form Equation for Predicting the Hydraulic Conductivity of Unsaturated Soils," *Soil Science Society of America Journal*, vol. 44, no. 5, pp. 892–898, Sep. 1980.

- [14] G. Capparelli and G. Spolverino, "An Empirical Approach for Modeling Hysteresis Behavior of Pyroclastic Soils," *Hydrology*, vol. 7, no. 1, p. 14, Mar. 2020.
- [15] G. Spolverino, G. Capparelli, and P. Versace, "An Instrumented Flume for Infiltration Process Modeling, Landslide Triggering and Propagation," *Geosciences*, vol. 9, no. 3, p. 108, Feb. 2019.
- [16] M. Del Prete, F. M. Guadagno, and A. B. Hawkins, "Preliminary report on the landslides of 5 May 1998, Campania, southern Italy," *Bulletin of Engineering Geology and the Environment*, vol. 57, no. 2, pp. 113–129, Sep. 1998.
- [17] P. De Vita and M. Nappi, "Regional Distribution of Ash-Fall Pyroclastic Soils for Landslide Susceptibility Assessment," in *Landslide Science and Practice*, C. Margottini, P. Canuti, and K. Sassa, Eds. Berlin, Heidelberg: Springer Berlin Heidelberg, 2013, pp. 103–109.

Numerical simulations of landslide physical model results

Sabatino Cuomo ¹

¹University of Salerno, Via Giovanni Paolo II, n. 132, Fisciano, Italy; +39089964231 (scuomo@unisa.it)

Abstract

Physical models are widely used in landslide research. They allow direct and accurate measurement of the main driving forces and features of the fundamental processes regulating a landslide. Physical modelling is principally used to: i) investigate specific or general landslide mechanisms, ii) validate mathematical formulations or numerical codes, iii) infer how a real in-situ slope and landslide scenario may evolve. This paper will provide some remarks on the first two issues. The FEM (Finite Element Method) and MPM (Material Point Method) analyses of a reduced-scale slope model that is gradually saturated by water table raising, is used as a benchmark. In this case, the experiment shows that the slope fails by shear and then liquefaction occurs, and numerical simulations can capture such slope instability sequence. On the other hand, flume tests of saturated granular flows are simulated via SPH (Smooth Particle Hydrodynamics) to interpret the spatio-temporal evolution of the pore water pressure within the rapid flow. An example of test regarding Landslide-Structure-Interaction is also proposed. The paper discusses the extent to which physical models and numerical simulations are complementary. The limitations of both types of approaches are also highlighted, such as scale-effects or computational costs.

Keywords: mechanisms, experimental, numerical

1 Introduction

There are several reasons that make the analysis of landslides a complex task. These include, for instance, multiple combined mechanisms, the strain-dependent behaviour of the involved soils, and the transient groundwater regime, especially in partially saturated soils and in fast-moving landslides. It is generally accepted that landslide recognition and diagnosis are the first two fundamental steps to be taken. Landslide recognition includes the assessment of site boundary conditions and the evolution of the slope over time. Landslide diagnosis involves relating the causes (factors) and the effects. These relationships are usually named mechanisms. The individuation of landslide mechanisms can be pursued at different scales, from regional/territorial to local/micro scales. Qualitative or quantitative, empirical or physically based interpretations are applicable depending on the general scope of the activities, for instance, land-use planning or design of protection structures. In the most complex cases, landslide physical modelling is a powerful tool for direct observation of landslide mechanisms. An undoubtable advantage is the high accuracy of the measurements it allows. Nevertheless, a simplification of the site stratigraphy and geometrical conditions is always required. Another important limitation concerns the reduced dimensions of the landslide model compared to the site problem. In this sense, scale effects can be opportunely managed, and even much reduced if a centrifuge device is used. Independent on the type of physical model, its combination with geomechanical numerical simulations has proven to be efficient for an advanced landslide diagnosis. This paper reports 4 emblematic cases, where complex scientific questions could be answered thanks to the combined use of physical and numerical landslide models.

2 Failure first, then liquefaction: a lesson learnt

2.1 Experimental results

The scientific question was: Is static liquefaction of soil the only cause of flow-like landslides? In other words, is liquefaction the cause or the effect of a slope instability when a flow-like landslide occurs? Eckersley [1] and several later slope model results (including [2]) have demonstrated that a slope model of loose material subjected to a rise in the groundwater table (eventually in conjunction with water inflow from the ground surface) first fails, then liquefaction occurs, and finally a retrogressive slope instability is initiated (Fig. 1). Images of slope instabilities observed through transparent side walls and measurements of pore water pressure at different points inside the slope were supported this explanation. The interested readers may refer to the references given.

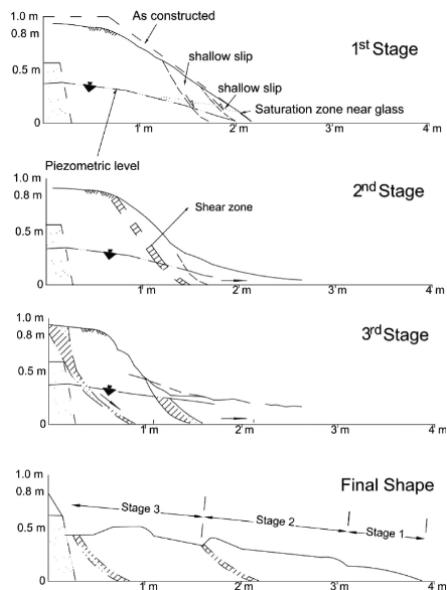


Figure 1: Experimental results of one flume test of Eckersley [1]: failure and post-failure stages.

2.2 Small-deformation FEM modelling

How to confirm these experimental results via numerical modelling? Analyses based on no-deformation or small-deformation approaches could be used. Definitions and examples are reported in Cuomo et al. [3](2021a). For instance, while it is not possible to simulate the slope multiple retrogression failures observed by Eckersley [1], static liquefaction is capturable if an advanced soil constitutive model is used. First, a simplified limit equilibrium analysis pointed out a slope safety factor close to one for a groundwater table equal to that observed at the occurrence of slope failure. This means that soil shear failure plays a role. Then, the liquefiable behaviour of the soil measured in undrained compression triaxial tests for different values of porosity was simulated by an advanced constitutive model based on Generalised Plasticity [4]. Some of these results are reported in Cascini et al. [5]. Finally, FEM analyses, based on a hydro-mechanical fully coupled approach, were performed. A series of numerical simulations carried out with the

GHM (GeHoMadrid) code [6] outlined that the failure of the toe of the slope can be simulated consistently to the flume test results. In conclusion, numerical modelling corroborated the experimental evidence in a physically based framework, which has been appropriately implemented in the numerical code.

2.3 Large-deformation MPM modelling

The same experiments have been simulated again some years later by Cuomo et al. [7]. As in the previous case, the geomechanical framework relied on full hydro-mechanical coupling and advanced constitutive modelling. The latter was based on the hypoplasticity theory [8]. However, this time the problem this time was casted in terms of large soil deformations and the numerical technique of the Material Point Method (MPM) was used by the Anura3D code. MPM is an enhancement of the classical FEM. The use of MPM in this context implies that both shear failure and subsequent liquefaction at the base of the slope could be captured. In addition, the spatio-temporal evolution of soil liquefaction on the slope was tracked, and the retrogressive type of the slope instability (Fig. 2) was captured [7]. It was demonstrated that static liquefaction is attained at the toe of the slope, which then largely deforms. Hence, a retrogressive landslide is triggered, which causes a lateral decompression and an increase in shear stress in the rear of the slope. Static liquefaction propagates backwards, thus triggering other multiple retrogressive failures. As the failed material propagates and finally comes to rest, global instability brings to the final flat deposit. What is the lesson learnt? The failure stage depends on the hydraulic boundary conditions. The post-failure stage, i.e., the transition of a slide into a flow, is regulated by soil static liquefaction. The later slope evolution until it stops is controlled by large deformations of the soil and the change in geometry.

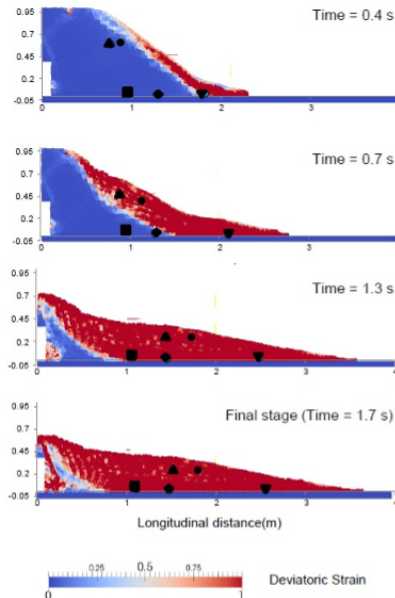


Figure 2: Displacements and deviatoric shear strains computed at different times by Cuomo et al. [7].

3 Loose and dense sands both prone to flow landslides?

3.1 Experimental results

A fundamental scientific question is that: soil behaviour or site condition, what is the most important factor? This issue is especially relevant for flow-like landslides, sometime called runaway landslides. It is agreed that loose, saturated sands may undergo static liquefaction and generate flowslides. However, from field observations, there are also known cases where the soils were not so loose but still suffered from slope instabilities that later evolved into flow-like landslides. Take et al. [9] provided convincing experimental evidence for the first time by using an unsaturated slope model in a centrifuge. A two-layer slope model was prepared, with coarser material at the top and finer material at the contact with the impervious bedrock. Displacements were measured with a high-speed camera and image processing, and pore water pressures with transducers embedded in the slope. A transient seepage was induced in the upper layer, leading to the formation of a perched water table at the top of slope (Fig. 3).

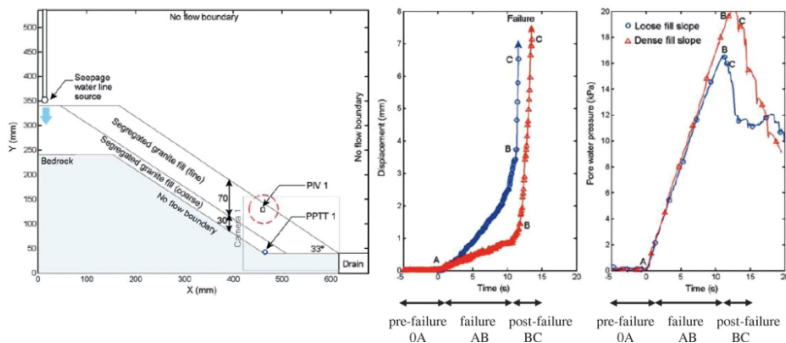


Figure 3: Centrifuge slope model for loose and dense soils: (a) centrifuge model scheme, (b) displacement measured at PIV1, and (c) pore-water pressures measured at PPTT1 (modified from Take et al. [9]).

The most-important evidence was that a flow-like landslide was triggered in the coarser material, regardless of soil density, either in the loose or dense case. This experimental evidence has important practical implications. It means that the chance for flow-like landslides in the field cannot be absolutely limited to the case of loose materials. Dense materials also deserve attention. However, how to explain such evidence from a geomechanical viewpoint?

3.2 FEM modelling

Both soil constitutive response (static liquefaction) and transient seepage (constrained in the layered slope stratigraphy) are the two key factors. This was the working idea of Cascini et al. [5]. The authors set up a numerical model corresponding to the prototype of the centrifuge tests of Take et al. [9]. The GHM (GeHoMadrid) code was used also in this case in combination with a Generalized Plasticity soil constitutive model [4], which can reproduce static liquefaction for loose sand. The main numerical outcomes can be summarized as follows: slope instability is simulated in both loose and dense slope models; the failed soil volumes are similar in the two cases; transient constrained seepage plays a role in both cases; however, in the dense slope model, localized failure occurs (a shear band starts at the toe of the slope and propagates backwards); in the loose slope model, diffuse failure due to static liquefaction occurs; failure is brittle for dense slopes and more delayed in time for loose ones.

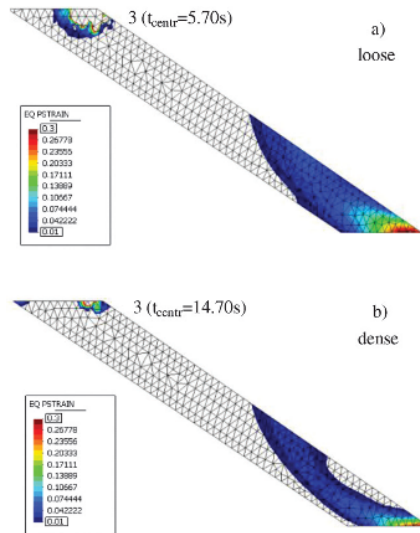


Figure 4: Time trend of the equivalent plastic strains computed for (a) loose and (b) dense soils by Cascini et al. [5].

4 Pore water pressure during propagation: new insights

4.1 Experimental results

Excess pore water pressures in fast-moving landslides are recognized as responsible for long runout distances travelled even along gentle piedmont areas. Small and (more recent) large flume tests have helped to understand how much interstitial fluid is important. When flow thickness, total weight and basal pore water pressures are measured at specific locations, information about a liquefied state (or not) of the flowing material can be obtained. In the experiments of Iverson et al. [10], such measurements were performed at the terminal part of an 80 m long flume. Pore water pressures close or equal to the total stress values were measured. It entails that the material is completely liquefied while propagating downslope. However, such high pore water pressures are dissipated during flow deposition.

4.2 SPH modelling

In this case, a large deformation framework is absolutely needed to reproduce the movement of the initial soil mass along the slider. However, the hydro-mechanical coupling of the soil is also fundamental. Among a series of approaches potentially applicable to this case, Cascini et al. [11] selected a compromise solution approach based on the following: hydro-mechanical coupled propagation approach; depth-integrated formulation instead of a 3D model; Smooth Particle Hydrodynamics (SPH) numerical tool to ensure fast computation with good numerical accuracy. Details about the used SPH formulation are given in Pastor et al. [12]. However, a SPH-FDM formulation [13] was also employed, which combines the SPH model with a 1D vertical FDM (Finite Difference Method) model for a more accurate evaluation of pore water pressures along the height of the flowing mass. Both formulations are available in the GeoFlowSPH code developed by Prof. Pastor and coworkers. In both models, a frictional rheological behaviour of soil was assumed with the pore water pressure computed separately. Fig. 6 shows the accurate reproduction of the measure-

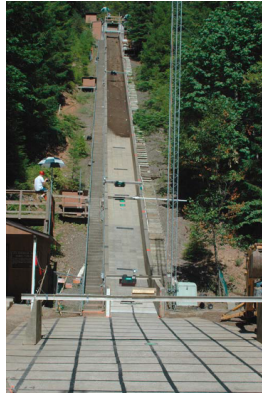


Figure 5: Photo of a 10 m³ debris flow tested in the USGS flume (from [10])

ments obtained along the slope at two different distances from the gate. Both the SPH and the SPH-FDM formulations were adequate to reproduce the observed behaviors.

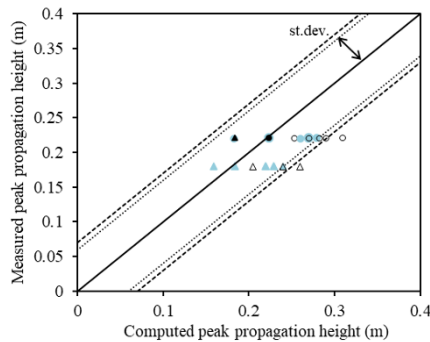


Figure 6: Experimental results versus numerical simulations. Measurements taken at 32 m (circles) and 66 m (triangles) from the gates. The mean values and standard deviation (σ) of the two set of measurements. Empty symbols: SPH model. Solid symbols: SPH-FDM model. (modified from Cascini et al. [11])

5 Landslide structure interaction: challenges for flows

5.1 Experimental results

Complementary to the previous debris flow flume experiments are those investigating the interaction of flows (dry or saturated) against walls, obstacles or structures, reproduced at reduced scale in flume or centrifuge tests. Song et al. [14] performed a series of centrifuge tests with saturated granular materials initially stored into a tank and then released through a bottom gate. The material flows downwards very rapidly and impacts against a fixed, rigid wall. In some cases, the material stops behind the wall; in other conditions, the flow overcomes the wall; even combined modes are observed. In all tests, the time-trend of lateral pressure exerted against the wall is measured at five locations along the wall. This provides complete

experimental evidence is for the so-called Landslide-Structure-Interaction (LSI).

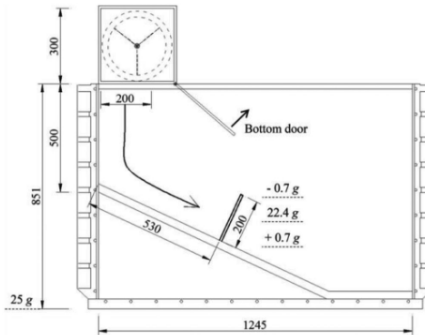


Figure 7: Centrifuge device used in the experiment of Song et al. [14]. All dimensions in millimetres.

5.2 MPM modelling

Modelling such complex behavior is not an easy task. It requires a formulation of large-deformations, a fully coupled hydro-mechanical approach, and efficient numerical algorithms to accurately reproduce such a dynamic problem (rapid propagation) and an impulsive action (impact against the wall). MPM modelling of these tests was proposed by Cuomo et al. [15] using a version of the Anura3D MPM code developed by Deltares (Delft, Netherlands), and a simple non-associative elasto-plastic constitutive model. Fig. 8 shows a time lapse where the material is extremely elongated, with the front part impacting the wall at about 20 m/s and the rear part of the flow not yet having moved from away from the bottom of the tank. Such numerical result is consistent with the experimental measurements. Interested readers can find details about the calibration and validation of the modelling approach in Cuomo et al. [15]. This demonstrates the capability of the numerical model to reproduce the complex geometrical configurations of the flow during the flow.

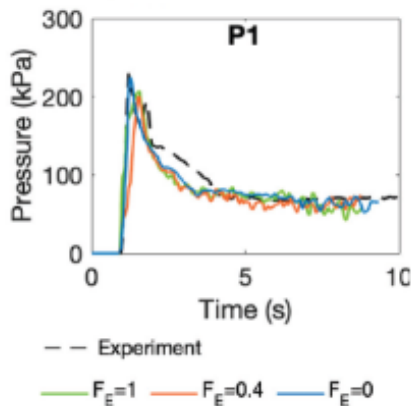


Figure 8: Example of velocity distribution for SL50 test run by Song et al. [14]. (Image modified from Cuomo et al. [15])

On the other hand, it is worth noting that the experimental centrifuge facility can reproduce such high (realistic) velocities well for the flow-structure impact scenarios. The dynamic behaviour of landslides is well simulated by the numerical modelling and, interestingly, the time-trends of the LSI are also well captured. For instance, Fig. 9 shows the experimental values of the impact pressure over time at the base of the wall compared to the numerical results. In this case, three different hypotheses for the Ergun coefficient [16], which regulates the non-linear contribution of the seepage velocity on the solid-liquid interaction forces (relevant in high porosity mixtures) are reported; and a negligible role of this factor is highlighted. In general, either the peak pressure or the subsequent drop over time is well captured by the modelling.

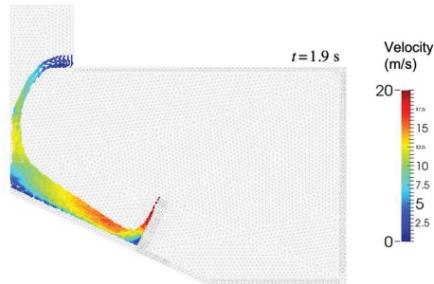


Figure 9: Experimental measurements and simulated values of the pressure at the impact zone for the SL50 test run by Song et al. [14]. (Image modified from Cuomo et al. [15])

6 Concluding remarks

The paper has presented 4 selected cases of landslide physical models: 2 flume tests (one with a length of 2 m for triggering, and another 80 m long used for propagation); and 2 centrifuge tests (one with a length of 0.6 m for triggering at $N=30$ times the gravity acceleration, and another 1.2 m long used for landslide-structure-interaction at $N=22$). In all cases, the size of the model (although amplified by N in the centrifuge tests) is smaller than the real site conditions. Thus, some scale effects are expected in comparison to the real landslide behaviour. Another important issue is the high complexity of the (i) landslide model and (ii) numerical model. The former strongly depends on the quality (accuracy and readiness) of the sensors, and an adequate slope geometry simplification is relevant as well. The latter relies on an appropriate geomechanical framework (equations to be solved), a robust numerical technique and a sound constitutive or rheological soil model. Based on the experience achieved so far, two combined analyses seem particularly well suited. i) Detailed field investigations combined with traditional geomechanical analyses of groundwater seepage and slope limit equilibrium conditions are especially useful to establish landslide diagnosis and recognition. ii) A physical model combined with numerical analysis is the next step to corroborate the landslide mechanisms identified by the field evidence and the analyses from step i).

Acknowledgements

Prof. Manuel Pastor and colleagues of the UPM (Universidad Politecnica de Madrid, Spain) are deeply acknowledged for the scientific support and for the permission to use the GeHoMadrid FEM code and different versions of the GeoFlow SPH code. The author is grateful to Dr. Mario Martinelli for the support in the MPM simulations, which were performed through the Anura3D code (<http://www.mpm-dredge.eu/>) and using also a version of Anura3D developed by Deltares (Delft, Netherlands). Colleagues from the University

of Salerno (Italy) are much acknowledged for the support in modelling and for several scientific discussions: Prof. Leonardo Cascini, Dr. Angela Di Perna, Dr. Pooyan Ghasemi, Dr. Ilaria Rendina and Dr. Claudia Sacco.

References

- [1] D. Eckersley, "Instrumented laboratory flowslides," *Géotechnique*, vol. 40, pp. 489–502, 9 1990.
- [2] S. D. Lourenço, K. Sassa, and H. Fukuoka, "Failure process and hydrologic response of a two layer physical model: Implications for rainfall-induced landslides," *Geomorphology*, vol. 73, pp. 115–130, 1 2006.
- [3] S. Cuomo, A. D. Perna, and M. Martinelli, "Material point method (mpm) hydro-mechanical modelling of flows impacting rigid walls," *Canadian Geotechnical Journal*, vol. 58, pp. 1730–1743, 11 2021.
- [4] M. Pastor, O. C. Zienkiewicz, and A. H. C. Chan, "Generalized plasticity and the modelling of soil behaviour," *International Journal for Numerical and Analytical Methods in Geomechanics*, vol. 14, pp. 151–190, 4 1990.
- [5] L. Cascini, S. Cuomo, M. Pastor, and C. Sacco, "Modelling the post-failure stage of rainfall-induced landslides of the flow type," *Canadian Geotechnical Journal*, vol. 50, pp. 924–934, 9 2013.
- [6] M. Pastor, J. A. F. Merodo, E. Gonzalez, P. Mira, T. Li, and X. Liu, "Modelling of landslides: (i) failure mechanisms," pp. 287–317, 2004.
- [7] S. Cuomo, P. Ghasemi, M. Martinelli, and M. Calvello, "Simulation of liquefaction and retrogressive slope failure in loose coarse-grained material," *International Journal of Geomechanics*, vol. 19, p. 04019116, 10 2019.
- [8] P.-A. von Wolfersdorff, "A hypoplastic relation for granular materials with a predefined limit state surface," *Mechanics of Cohesive-frictional Materials*, vol. 1, pp. 251–271, 7 1996.
- [9] W. A. Take, M. D. Bolton, P. C. P. Wong, and F. J. Yeung, "Evaluation of landslide triggering mechanisms in model fill slopes," *Landslides*, vol. 1, pp. 173–184, 9 2004.
- [10] R. M. Iverson, M. Logan, R. G. LaHusen, and M. Berti, "The perfect debris flow? aggregated results from 28 large-scale experiments," *Journal of Geophysical Research*, vol. 115, p. F03005, 7 2010.
- [11] L. Cascini, S. Cuomo, M. Pastor, and I. Rendina, "Sph-fdm propagation and pore water pressure modelling for debris flows in flume tests," *Engineering Geology*, vol. 213, pp. 74–83, 11 2016.
- [12] M. Pastor, B. Haddad, G. Sorbino, S. Cuomo, and V. Dremptic, "A depth-integrated, coupled sph model for flow-like landslides and related phenomena," *International Journal for Numerical and Analytical Methods in Geomechanics*, vol. 33, pp. 143–172, 2 2009.
- [13] M. Pastor, M. M. Stickle, P. Dutto, P. Mira, J. A. F. Merodo, T. Blanc, S. Sancho, and A. S. Benítez, "A viscoplastic approach to the behaviour of fluidized geomaterials with application to fast landslides," *Continuum Mechanics and Thermodynamics*, vol. 27, pp. 21–47, 1 2015.
- [14] D. Song, C. Ng, C. Choi, G. Zhou, J. Kwan, and R. Koo, "Influence of debris flow solid fraction on rigid barrier impact," *Canadian Geotechnical Journal*, vol. 54, pp. 1421–1434, 10 2017.

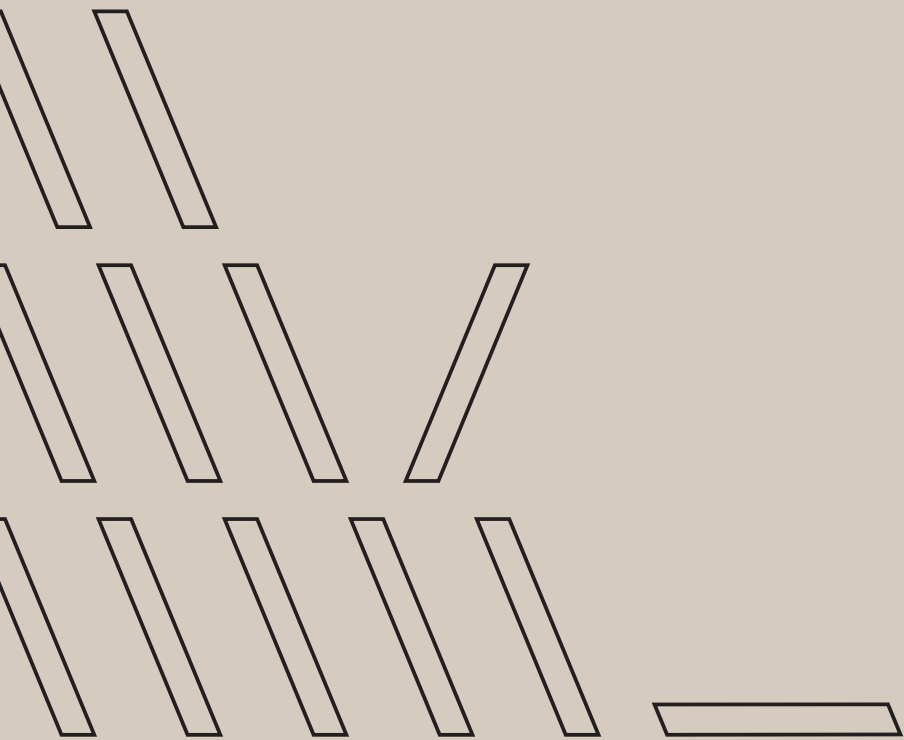
- [15] S. Cuomo, A. D. Perna, and M. Martinelli, "Material point method (mpm) hydro-mechanical modelling of flows impacting rigid walls," *Canadian Geotechnical Journal*, vol. 58, pp. 1730–1743, 11 2021.
- [16] Ergun and S., "Fluid flow through packed columns," *Chem. Eng. Prog.*, vol. 48, pp. 89–94, 1952.

List of Project publications

- Željko Arbanas, Sara Pajalić, Vedran Jagodnik, Josip Peranić, Martina Vivoda Prodan, Petra Đomlija, S Dugonjić Jovančević, and Nina Čeh. Development of physical model of landslide remedial constructions' behaviour. In *Proceedings of 4th regional symposium on landslides in Adriatic Balkan Region, Sarajevo, Bosnia and Herzegovina*, pages 23–25, 2019.
- Željko Arbanas, Vedran Jagodnik, Josip Peranić, Sara Pajalić, Martina Vivoda Prodan, and Nina Čeh. Physical model of rainfall induced landslide in flume test: preliminary results. In *Proceedings of 4th European conference on physical modelling in geotechnics. Lulea University of Technology*, 2020a.
- Željko Arbanas, Josip Peranić, Martin Krkač, Vedran Jagodnik, Petra Jagodnik, and Srnežana Mihalić Arbanas. Report of the IPL-219, IPL-220 and Croatian WCoE 2017–2020: From Landslide Investigation to Landslide Prediction and Stabilization. In *Workshop on World Landslide Forum*, pages 281–291. Springer, 2020b.
- Vedran Jagodnik, Petra Đomlija, Katarina Oštrić, and Željko Arbanas. Strength reduction curve of soils from eluvial deposits in Vinodol Valley, Croatia. In *Proceedings of the 4th regional symposium on landslides in the Adriatic—Balkan region. Društvo za geotehniku u Bosni i Hercegovini*, pages 109–114, 2019.
- Vedran Jagodnik, Josip Peranić, and Željko Arbanas. Mechanism of landslide initiation in small-scale sandy slope triggered by an artificial rain. In Željko Arbanas, Peter T. Bobrowsky, Kazuo Konagai, Kyoji Sassa, and Kaoru Takara, editors, *Understanding and Reducing Landslide Disaster Risk: Volume 6 Specific Topics in Landslide Science and Applications*, ICL Contribution to Landslide Disaster Risk Reduction, pages 177–184. Springer, 2020.
- Sara Pajalić, Vedran Jagodnik, and Željko Arbanas. Physical model for testing the behavior of landslide remediation constructions. In *7th Regional Conference: "Zajednički temelji"*, pages 37–42, 2019. in Croatian.
- Sara Pajalić, Josip Peranić, Sandra Maksimović, Nina Čeh, Vedran Jagodnik, and Željko Arbanas. Monitoring and data analysis in small-scale landslide physical model. *Applied Sciences*, 11(11):5040, 2021.
- Josip Peranić and Željko Arbanas. Impact of the wetting process on the hydro-mechanical behavior of unsaturated residual soil from flysch rock mass: preliminary results. *Bulletin of Engineering Geology and the Environment*, 79(2):985–998, 2020.
- Josip Peranić, Mariagiovanna Moscariello, Sabatino Cuomo, and Željko Arbanas. Determination of hydraulic conductivity and shear strength properties of unsaturated residual soil from flysch rock mass. In *E3S Web of Conferences*, volume 195, page 03022. EDP Sciences, 2020a.

Josip Peranić, Mariagiovanna Moscariello, Sabatino Cuomo, and Željko Arbanas. Hydro-mechanical properties of unsaturated residual soil from a flysch rock mass. *Engineering Geology*, 269:105546, 2020b.

Josip Peranić, Snježana Mihalić Arbanas, and Željko Arbanas. Importance of the unsaturated zone in landslide reactivation on flysch slopes: observations from Valiči Landslide, Croatia. *Landslides*, 18(12):3737–3751, 2021.



Project *Physical modelling of landslide remediation constructions behaviour under static and seismic actions* (IP-2018-01-1503)

Physical modelling of landslide using scaled landslide models behaviour was established at the end of 1980s when in a scaled physical model (flume or flume test) behaviour of flowslide and liquefaction of sliding material were investigated. The main task of landslide physical modelling in last 25 years was research of initiation, motion and accumulation of fast flow like slides caused by infiltration of surface water in a slope. The numerous established landslide physical models and researches can be divided in two main groups related to landslide main triggering factors: rainfall and earthquakes. The existing studies of landslide remedial construction behaviour using physical modelling are very rare. The proposed Project will encompass researches of behaviour of different construction applied for landslide remediation in physical models of scaled landslides in static and dynamic conditions where static conditions imply conditions for rainfall triggered landslides and dynamic conditions imply conditions for earthquake induced landslides. Observations of landslide movements in a physical model will be carried out by sensor network for measuring displacements, pressures, forces and pore pressures and innovative photogrammetric equipment including terrestrial laser scanner and infrared camera. Scaled remedial constructions will be constructed by 3D printer that will enable precise scaled construction elements. The measured parameters from physical model will be included in 3D numerical simulation. The results of both physical and numerical modelling will enable better understanding of landslide remedial construction behaviour. Methods of stability analysis used for landslide remediation design in engineering practice are still very rough and result with selection of conservative remedial constructions. For that reason, research results would represent the base for new approaches to the rational landslide remedial construction designing in engineering practice.

The Project is funded by

Croatian Science Foundation, IP-2018-01-1503

